Waste Management 216 (2026) 115470

Contents lists available at ScienceDirect

Waste Management

journal homepage: www.elsevier.com/locate/wasman

Surfactant-Activated pharmaceutical waste biomass for efficient removal of Basic Violet 14: Experimental Investigation, Machine-Learning Optimization, and mechanistic validation by DFT calculations

Amira Othmani [a,*], Ibtissam Hammouche [a,b], Ammar Selatnia [a], Nasma Bouchelkia [c,d]

[a] Department of Chemical Engineering, Ecole Nationale Polytechnique, BP 182 El Harrach 16200 Algiers, Algeria
[b] Chemical Engineering Department, Abu Dhabi University, Abu Dhabi P.O.Box.No.59911, United Arab Emirates
[c] Laboratoire de Gestion et Valorisation des Ressources Naturelles et Assurance Qualité, Faculté SNVST, Université de Bouira, Bouira 10000, Algeria
[d] Centre de Recherche en Technologies Agro-Alimentaires, Route de Targa Ouzemmour, Campus Universitaire, Bejaia 06000, Algeria

ARTICLE INFO

Keywords:
Biosorbent valorization
Surfactant-modified biomass
Dye adsorption
Hybrid ANN optimization
DFT mechanistic validation

ABSTRACT

Dyes are extensively employed in the pharmaceutical industry and laboratories and their persistence in wastewaters presents severe environmental and health hazards due to toxicity and resistance to biodegradation. This study examines an efficient method of dye removal by valorization of pharmaceutical waste, *Streptomyces rimosus* (SR) biomass, raw and impregnated with SDS. The biosorbents were evaluated for removal of Fuchsin dye (Basic Violet 14, BV14) under varying pH, biosorbent dose, contact time, initial dye concentration, and temperature. SDS-SR showed ~ 98% removal at 2 g/L compared to 4 g/L for raw SR to have similar efficiency. Kinetic data were described by the pseudo-second order model and equilibrium data was described by Hill and Sips isotherms suggesting the presence of heterogeneous surfaces, cooperative adsorption and multilayer formation. Thermodynamic analysis confirmed a spontaneous ($\Delta G^\circ < 0$), exothermic ($\Delta H^\circ < 0$) physisorption-driven process. DFT calculation results showed that the SDS modification enhanced the BV14 adsorption energy from −1.42 to −2.87 eV, leading to an increase of the electrostatic and hydrophobic interactions which are consistent with experimental observations. Additionally, machine learning models (ANN, linear regression, decision tree, random forest) were trained on experimental data where ANN model resulted in the highest predictive accuracy. Hybrid optimization using ANN couple with GA and PSO was used to find optimal operational conditions for maximum adsorption. This study proves that SDS-modified SR is an effective and eco-friendly biosorbent as it combines waste valorization and molecular-level understanding using DFT with predictive AI modeling. The approach offers a sustainable, circular-economy strategy for pharmaceutical and laboratory wastewater treatment, combining high removal efficiency, mechanistic insight, and data-driven optimization.

1. Introduction

Pharmaceutical and laboratory industries are major contributors to complex industrial wastewater, with pharmaceutical manufacturing processes producing several hundred to several thousands of cubic meters of effluent per ton of product, which is of great challenge for conventional treatment. These effluents contain various organic and inorganic contaminants such as synthetic dyes, solvents, antibiotics and other biologically active compounds, which are often resistant to degradation (Bharagava et al., 2020). Among them, cationic dyes like Basic Fuchsin, or Basic Violet 14 (BV14), are commonly seen in biological staining, diagnostic assays and laboratory uses, and can be released to aquatic systems through laboratory, pharmaceutical and mixed industrial discharges (El-Sayed et al., 2024; J. Griffiths., 1984). Their intense color, high solubility and chemical stability make them very persistent in the aquatic environment, and their aromatic structures resist conventional biodegradation processes, resulting in ecological and human health risks (Patil et al., 2022; Singha et al., 2021).

* Corresponding author.
E-mail addresses: amira.othmani@g.enp.edu.dz (A. Othmani), ibtissam.hammouche@g.enp.edu.dz (I. Hammouche), ammar.selatnia@g.enp.edu.dz (A. Selatnia), nasma.bouchelkia@crtaa.dz (N. Bouchelkia).

https://doi.org/10.1016/j.wasman.2026.115470
Received 13 January 2026; Received in revised form 25 February 2026; Accepted 10 March 2026
Available online 18 March 2026
0956-053X/© 2026 Elsevier Ltd. All rights are reserved, including those for text and data mining, AI training, and similar technologies.

Conventional wastewater treatment approaches, such as coagulation, flocculation, membrane filtration, activated carbon adsorption and biological degradation, are not always effective in removing these dyes, due to their low biodegradability and possible microbial toxicity (Islam et al., 2022; Slama et al., 2021). Physicochemical techniques such as oxidation and ozonation, although they are great for degrading the organic molecules, are energy-intensive, and may produce harmful by-products. Consequently, sustainable alternatives are required to address dye-laden wastewater effectively.

Biosorption has emerged as a promising solution, using natural materials with high functional groups that can bind dye molecules (Chan et al., 2022; Deyris et al., 2023; do Nascimento Júnior et al., 2024; Okoro et al., 2022), which are cost-effective, environmentally friendly and easy to implement, especially from waste biomass (do Nascimento Júnior et al., 2024; Elgarahy et al., 2021; Guleria et al., 2022; Sharma et al., 2022). Various biosorbents obtained from agricultural residues, microbial biomass, and industrial by-products (Azeez and Al-Zuhairi, 2022; Sintakindi and Ankamwar, 2021; Tang et al., 2022) have shown high adsorption capacities for dyes such as methyl violet 2B (Kooh et al., 2018), malachite green (Kooh et al., 2016) and rhodamine B (Kooh et al., 2019). Moreover, the development of green photocatalysts based on agricultural wastes offers the twin advantage of efficient dye degradation and valorization of biomass waste (Asim et al., 2022; Khan et al., 2023).

Building on this basis, the current study examines the potential of *Streptomyces rimosus* (SR) biomass, a by-product of the production of antibiotics, as a novel bioremediant for the removal of BV14. To improve the adsorption performance, SR biomass was surface modified using sodium dodecyl sulfate (SDS), an anionic surfactant that can introduce new functional groups, increase the hydrophobicity (Almas et al., 2023) facilitate and increase electrostatic interactions (Sharma et al., 2024) with cationic dyes (Naseem et al., 2022). Previous studies with SDS modified biosorbents such as rice husk and chitosan have demonstrated enhanced adsorption of dyes such as crystal violet (Ahmad et al., 2022) and methylene blue (Ranjbari et al., 2022). Thus, SDS treatment is hypothesized to significantly enhance the BV14 removal efficiency of SR biomass (Saxena et al., 2023).

Recently, machine learning (ML) techniques have become prominent in the field of environmental engineering because they can be used to model complex nonlinear systems and optimize process conditions. In this study, experimental biosorption data were modeled by ANN (Taoufik et al., 2022), linear regression (Yang et al., 2021), decision tree (Hassan and Kazemi, 2025), and random forest (Zhao et al., 2024) algorithms, whereas hybrid optimization techniques (GA and PSO) (Khiam et al., 2022; C. Li et al., 2024) were used to determine the optimum operational parameters, integrating experimental data with predictive modeling for better process understanding (Gamboa et al., 2024).

To elucidate the adsorption mechanisms, the effects of initial pH, kinetics, isotherms and thermodynamics were systematically studied. Additionally, density functional theory (DFT) was used to compare the interaction energies of BV14 with raw and SDS modified biomass surfaces to validate experimental data on a molecular level. This approach not only confirms the reliability and precision of the experimental data but also demonstrates the feasibility of using DFT as a predictive tool for guiding biosorbent selection and process design prior to labor-intensive experimentation.

The novelty of this work lies in the integrated investigation of BV14 removal using a valorized pharmaceutical by-product, *Streptomyces rimosus* biomass, activated through SDS surfactant modification. Experimental results were modeled and optimized using bi-hybrid machine learning approaches (ANN–GA and ANN–PSO), while DFT calculations provided molecular-level insight and validated experimental precision, highlighting the potential of DFT as a predictive tool for future biosorption studies. This multidisciplinary approach advances fundamental understanding and offers a sustainable, data-driven strategy for treating pharmaceutical and laboratory wastewater within a circular economy framework.

2. Materials and methods

2.1. Materials and chemicals

The following materials and chemicals were used in this study:

- Biomass: Mycelial biomass of *Streptomyces rimosus* (SR), obtained as a by-product from the SAIDAL pharmaceutical unit (Médéa, Algeria), where it is used for oxytetracycline production. In its raw state, the biomass appears as superposed brown sheets (Finlay et al., 1950).
- Surfactant: Sodium dodecyl sulfate (SDS), analytical grade, purchased from Sigma-Aldrich (Table S1).
- Adsorbate: Fuchsin dye (Basic Violet 14, BV14), analytical grade, obtained from Sigma-Aldrich (Table S1).
- Other chemicals: Potassium nitrate (KNO_3), hydrochloric acid (HCl, 0.1 N), and sodium hydroxide (NaOH, 0.1 N) were used for pH adjustments and pH_pzc determination. All chemicals were of analytical grade and used without further purification.
- Water: Distilled water was used for all solution preparations and washing steps.

2.2. Adsorbent preparation and surfactant impregnation

The raw SR biomass was thoroughly washed with tap water, followed by distilled water, and dried in an oven at 55 °C for 24 h until a constant weight was achieved. The dried biomass was mechanically ground and sieved to obtain a granulometry size ranging from 50 to 160 µm.

To prepare SDS-impregnated SR biomass (SDS-SR), 20 g of SDS was dissolved in 250 mL of distilled water and mixed with 10 g of SR biomass under continuous agitation for 24 h (Chatterjee et al., 2011). The resulting suspension was vacuum-filtered, and the collected biomass was dried at 55 °C for 24 h, then ground and sieved to 50–160 µm (Ahmad et al., 2022; Ranjbari et al., 2022).

2.3. Determination of the point of zero charge (pH_{PZC})

The point of zero charge (pH_{PZC}) indicates the pH at which the adsorbent surface is electrically neutral when introduced into a solution. It represents the pH at which the biomass surface has zero charge.

To determine the pH_{PZC}, 50 mL of 0.1 M KNO_3 solution was placed in a series of 250 mL Erlenmeyer flasks, whose initial pH was adjusted between 2 and 10 by adding either 0.1 N HCl or 0.1 N NaOH (Feddane et al., 2023). 1 g of either SR biomass or SDS-SR biomass was added to each flask. The solid liquid mixture was continuously stirred for 48 h, after which the final pH of each solution was measured (Ahamad and Nasar, 2024).

The variation between the initial and final pH values was then plotted against the pH_i. pH_{PZC} of SR or SDS-SR biomass is the intersection of the $\Delta pH(pH_f - pH_i) = f(pH_i)$ curve with the x-axis.

2.4. Adsorbate preparation

A stock solution of Fuchsin dye; also known as Basic Violet 14 (BV14) (Kim et al., 2025); was prepared at a concentration of 1000 mg/L by dissolving 1 g of dye in 1 L of distilled water. Working solutions with concentrations ranging from 10 to 250 mg/L were then obtained by appropriately diluting the stock solution with distilled water.

2.5. Batch experiments study

A calibration curve, A = f(C), was prepared using standard Fuchsin dye (BV14) solutions at known concentrations (2, 4, 6 …20 mg/L). The

absorbance of each solution was measured using a UV–visible spectrophotometer (Jenway 6700) at the maximum wavelength (λ_{max}) = 542 nm. This calibration curve was subsequently used to determine the concentration of unknown dye sample.

Batch adsorption experiments were carried out to evaluate the removal of BV14 by the biomass. In each experiment, 50 mL of dye solution with a known initial concentration (C_i) was placed in a 250 mL Erlenmeyer flask, and the initial pH (pH_i) was adjusted to the desired value using 0.1 N HCl or 0.1 N NaOH. A precisely weighed mass of biomass (m) was then added, and the mixture was stirred at 250 rpm at room temperature (297 K) for a predetermined contact time.

After the contact time, the biomass was separated from the solution by filtration through a 0.45 μm syringe filter, followed by centrifugation. The concentration of BV14 in the filtrate was determined using the UV–visible spectrophotometer at λ_{max} = 542 nm.

The amount of BV14 adsorbed at equilibrium or at t time was calculated using the following equation:

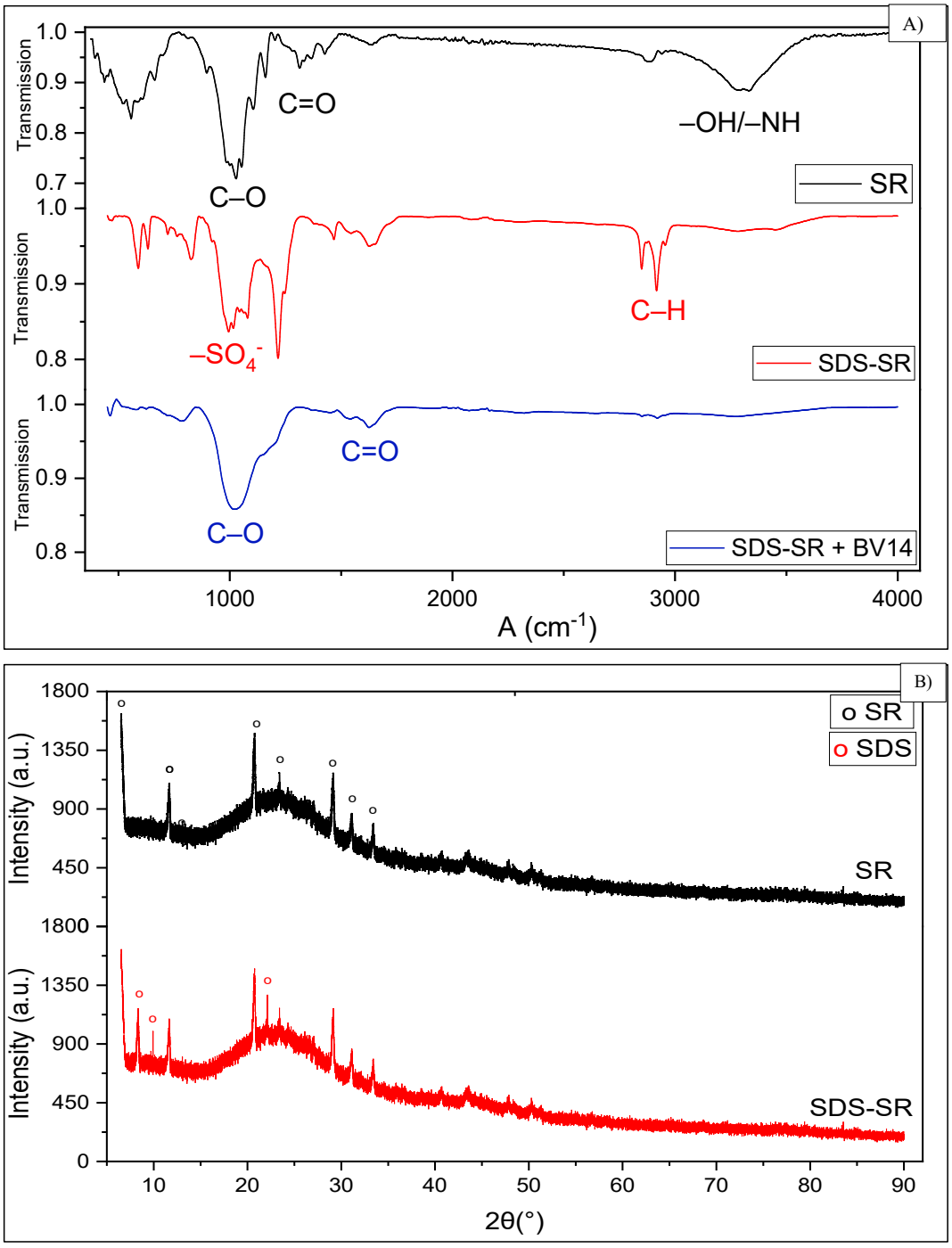

Fig. 1. A) Infrared spectrum of SR, SDS-SR before and after BV14 biosorption. B) X-ray Diffraction Spectroscopy. C) X-ray Photoelectron Spectroscopy. D) Thermogravimetric analysis. E) Brunauer-Emmett-Teller isotherm plots. F) Scanning Electron Microscopy of SR biomass before and after BV14 biosorption.

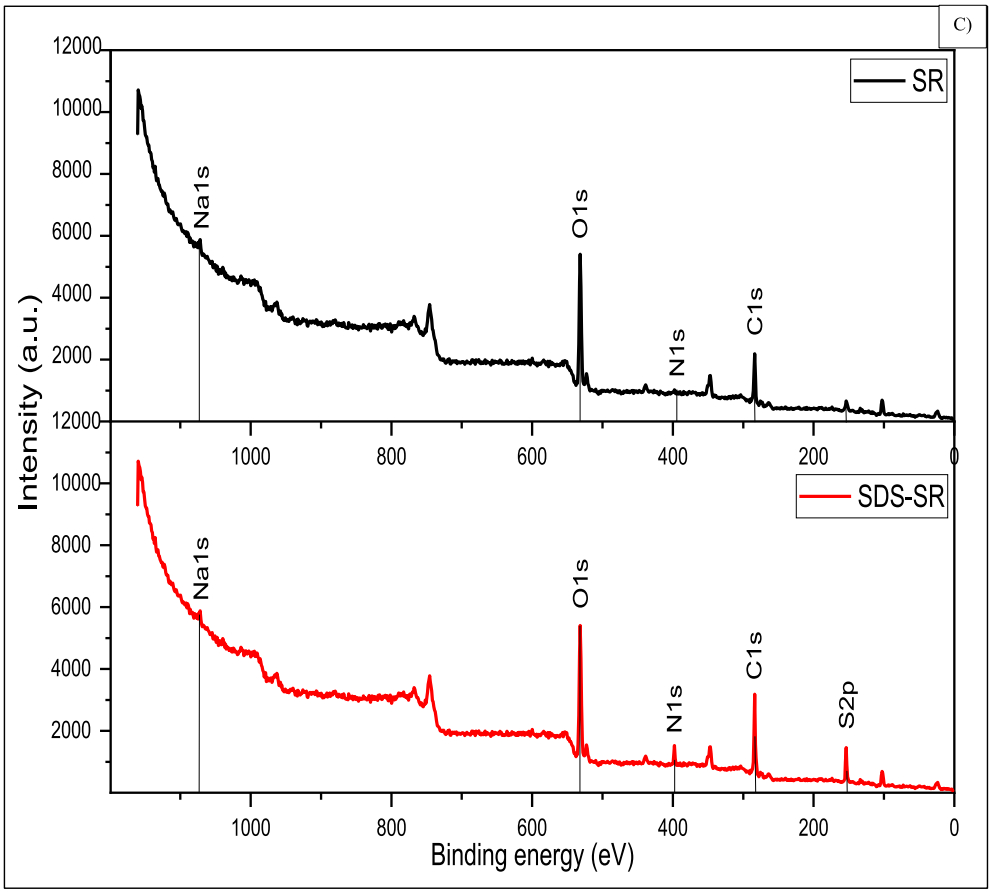

Fig. 1. (*continued*).

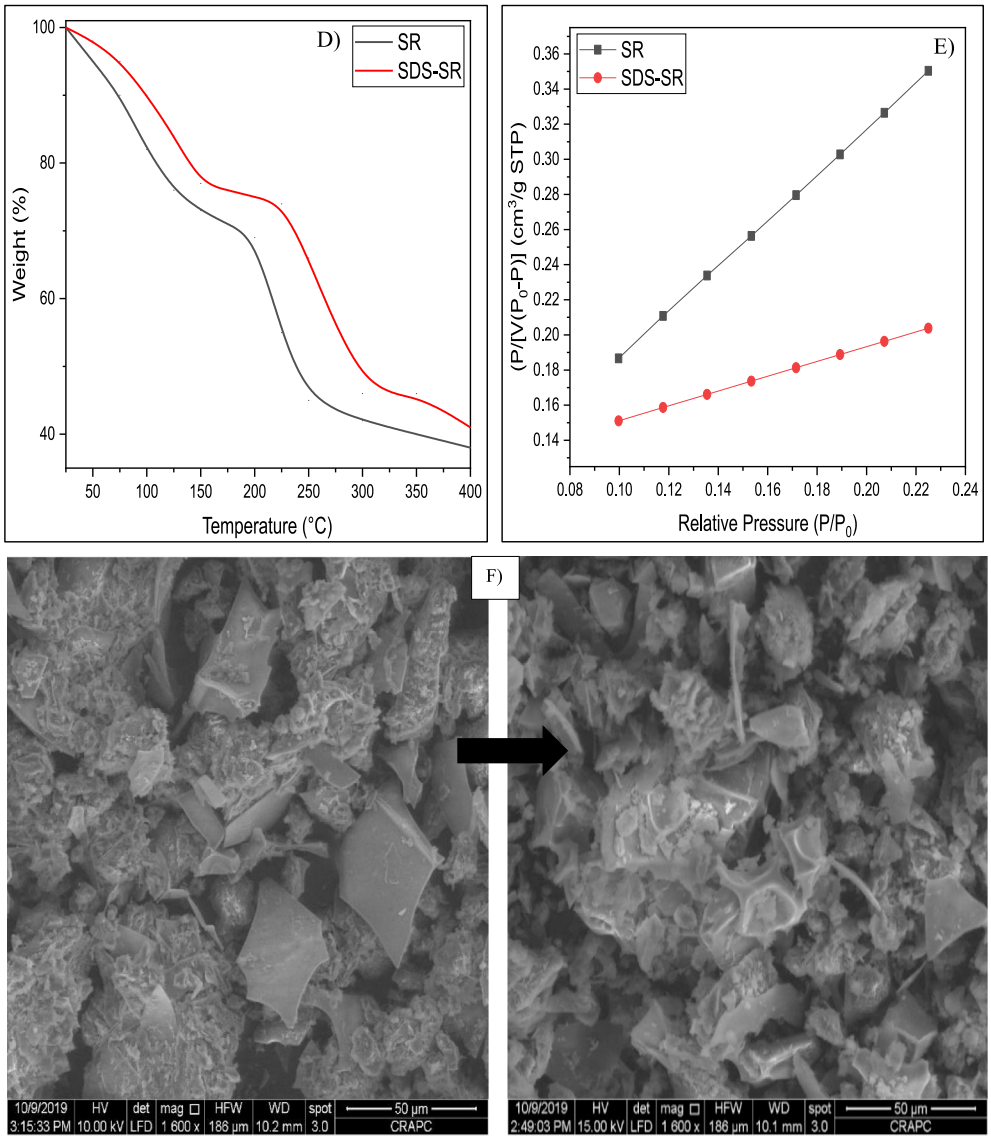

Fig. 1. (*continued*).

$$q_{e,t} = \frac{(C_i - C_{e,t})*V}{m} \quad (1)$$

and the removal percentage of BV14 was calculated using the following equation:

$$R(\%) = \frac{C_i - C_e}{C_i} \times 100 \quad (2)$$

Where C_i and C_e (mg/L) represent the initial and equilibrium BV14 concentrations, respectively; V (L) is the volume of BV14 solution; m (g) is the mass of the biomass; and q_e (mg/g) indicates the amount of BV14 adsorbed per gram of biomass at equilibrium.

2.6. Adsorption kinetics modeling

The adsorption kinetics of BV14 onto both SR and SDS-SR biomasses were investigated using the pseudo-first-order model (Lagergren, 1898) and the pseudo-second-order model (Ho and McKay) (Ho and Mckay, 1999). The corresponding kinetic equations, along with their rate constants are presented in table S2.

Comparing both models helps distinguish between physisorption which is dominated by physical attraction or chemisorption, which involves chemical bonding through electron sharing or exchange with surface functional groups (Jawad et al., 2019). This distinction is crucial to understand the nature of interactions between the biosorbent and the dye molecules.

2.7. Adsorption isotherm modeling

In order to model the experimental equilibrium data, eight different adsorption isotherm equations were evaluated to identify the best-fitting model. For this purpose, a nonlinear regression analysis based on the correlation coefficient was performed, together with two additional non-linear error analysis functions. The isothermal equations used in this study are summarized in table S2.

2.8. Adsorption thermodynamics

The change in Gibbs free energy ΔG during the adsorption process is connected to the adsorption equilibrium constant through the classical Van't Hoff equation in table S2 (Tran et al., 2021).

The value of the enthalpy change ΔH and the entropy change ΔS were determined from the slope and intercept, respectively, of the graph plotting ln (K°) versus1/T.

A full error analysis was performed to determine the most appropriate isothermal model, the three error functions (Nebaghe et al., 2016; Sivarajasekar and Baskar, 2019) used being presented in table S2.

2.9. Desorption study

Desorption and regeneration experiments (Ghosh et al., 2023) were conducted to assess the reusability of both SR and SDS-SR biomasses for the removal of BV14 dye. Adsorption experiments were carried out under the following conditions: initial dye concentration (C_i) = 20 mg/L, initial pH (pH_i) = 5, and biomass concentration (C_b) = 4 g/L for SR and 2 g/L for SDS-SR, at a constant room temperature of 297 K. The total adsorption removal percentage (Ads %) was then determined.

After adsorption, the biomass was separated via filtration, thoroughly washed with distilled water to remove unadsorbed dye residues, and dried for desorption analysis. Chemical regeneration was employed for the desorption studies. A methanol–water washing solution was prepared by mixing 2 mL of pure methanol with 8 mL of distilled water in a 50 mL Erlenmeyer flask. Then, a known quantity of dye-loaded biomass (1 g/L) was added to the flask, the assembly was stirred for 60 min at 250 rpm using a magnetical stirrer to ensure homogenization of the mixture.

Following stirring, the mixture was filtered and centrifuged, and the concentration of the desorbed BV14 dye was measured using a UV–Visible spectrophotometer (Jenway 6700) at a wavelength λ_{max} = 542 nm. The filtered biomass was then prepared for another adsorption–desorption cycle. A total of four consecutive adsorption–desorption cycles were performed. After each cycle, the amount of desorbed dye was quantified, and the desorption efficiency (%) was calculated using the following equation (Alsaiari et al., 2022):

$$\text{Des}\,(\%) = \left(\frac{C_d{}^{*}V_d}{q_e{}^{*}m}\right) \times 100 = \frac{q_d}{q_e} \times 100 \tag{3}$$

C_d (mg/L) is dye concentration in the desorbing solution, V_d (L) is the volume of the desorbing solution, q_e (mg/g) is the adsorption capacity obtained from the previous adsorption cycle, m (g) is the mass of biomass.

2.10. Density functional theory (DFT) Calculations

All DFT calculations were performed using the Gaussian 09 package with the B3LYP functional and 6-31G+(d,p) basis set (Yılmaz, 2025). Geometry optimizations as well as frequency analyses confirmed that all structures are true minima (Rad et al., 2021). Adsorption systems were built by placing the individual BV14 dye molecule in proximity to functional groups of two surface models:

(1) **a lipoteichoic acid (LTA) fragment**, representing the native cell-wall structure of raw *Streptomyces rimosus* (SR), and (2) **LTA impregnated with a SDS unit**, representing the SDS-impregnated biomass (SDS-SR) in different orientations (π-π stacking, hydrogen bonding and electrostatic interactions) (Tao et al., 2019). The most stable configurations were found by comparing the total adsorption energies calculated as (Sharma et al., 2023):

$$Eads = EBV14 + biomass - (EBV14 + Ebiomass) \tag{4}$$

and more negative values indicate stronger and more spontaneous interactions (Ibrahim et al., 2024). Frontier molecular orbitals (HOMO-LUMO) (Yen et al., 2017)(Ormachea et al., 2015), molecular electrostatic potential (MEP) maps (Vanasundari et al., 2017) and the conceptual DFT descriptors (chemical potential μ, hardness η, softness S, electrophilicity ω, and nucleophilicity N) were analyzed in order to describe the charge transfer, reactivity and local adsorption sites (Domingo et al., 2007). Parr functions (P_k^+ and P_k^-) were also calculated to find the electrophilic and nucleophilic regions participating in the adsorption (Zeng et al., 2017). This combined energetic and electronic analysis gives an integrated insight into the stability, strength and nature of dye-biomass interactions.

2.11. Machine learning methods

In this study, in order to predict the adsorption capacity of BV14 dye by SR and SDS-SR biomasses, four-machine learning methods were applied (artificial neural network, linear regression, decision tree, and random forest). Five features have been used, including the contact time, adsorbent concentration, initial dye concentration, pH, and temperature. The target output for all models was the adsorption capacity in (mg/g).

In order to check the model's effectiveness and generalization, the dataset was randomly split into 80% for training and 20% for testing for all methods. In order to validate the model performance, three standard metrics have been used: the correlation coefficient (R), the coefficient of determination (R2), and the root mean square error (RMSE), computed for training, testing, and all data combined.

Artificial Neural Networks (ANNs) (Fig. S1. A) are powerful machine learning methods that are known for being able to model complicated nonlinear relations (Tealab, 2018). Similar to biological neurons, ANNs use connected nodes to transmit and work on information. It is consisted of input, output, and hidden layers. Hidden layers contain the tunable number of nodes (Wu, 1992). The right selection of hidden nodes is necessary to avoid overfitting or underfitting. Overfitting is associated with too many features, whereas underfitting is caused by a not-complex-enough model. The use of cross-validation, regularization, and early stopping makes it possible to prevent overfitting and increase how well the model performs in general. In the current paper, a neural network with 1 hidden layer was trained using gradient descent with momentum to boost efficiency and stability.

Over time, linear regression has undergone many improvements in statistics. In the beginning, when computers were not available, it was common to linearize models by adjusting equations in a simple way. Linear regression is a method that explains the link between a dependent variable and one or more independent variables by finding the right coefficients from the data (Mostoufi and Constantinides, 2023). It supports statistical analysis and allows for expanding it with statistic techniques such as multiple linear regression for several independent variables (Li Haksun, 2022). Additionally, it has led to the development of the generalized linear model and hierarchical linear model (Yin et al., 2022).

A Decision Tree is a supervised learning algorithm that is applied to both regression and classification (Fig. S1. B). It organizes the data by splitting them using different feature values, which creates a tree structure with the root node at the top and the leaf nodes where predictions are done. Every time a split happens, it forms a rule that helps the model process the data. Interpreting decision tree is easy, and are able to deal with nonlinear relationships. However, overfitting can occur regularly, mostly if the dataset is small or has lots of noise. To overcome this, branches that are not needed are removed with pruning, which increases how well the model can generalize new data.

Random forest gathers and uses numerous decision trees, improving the model's precision and steadiness by mixing the outcomes predicted by each tree (Fig. S1. C). When making random selections of samples and features during RF development, the classifiers are more diverse, so the RF performs better in classification (Wang et al., 2024; Xia et al., 2024). RF uses the Bagging method, which is a parallel way of applying ensemble learning (Wang et al., 2022). Random noise in both columns and rows helps RF regression lower the odds of overfitting. The key principle in Bagging is to get several samples from the original sample using the Bootstrap method, develop a decision tree for each sample, and combine all their predictions by voting (Dar and Chand, 2024).

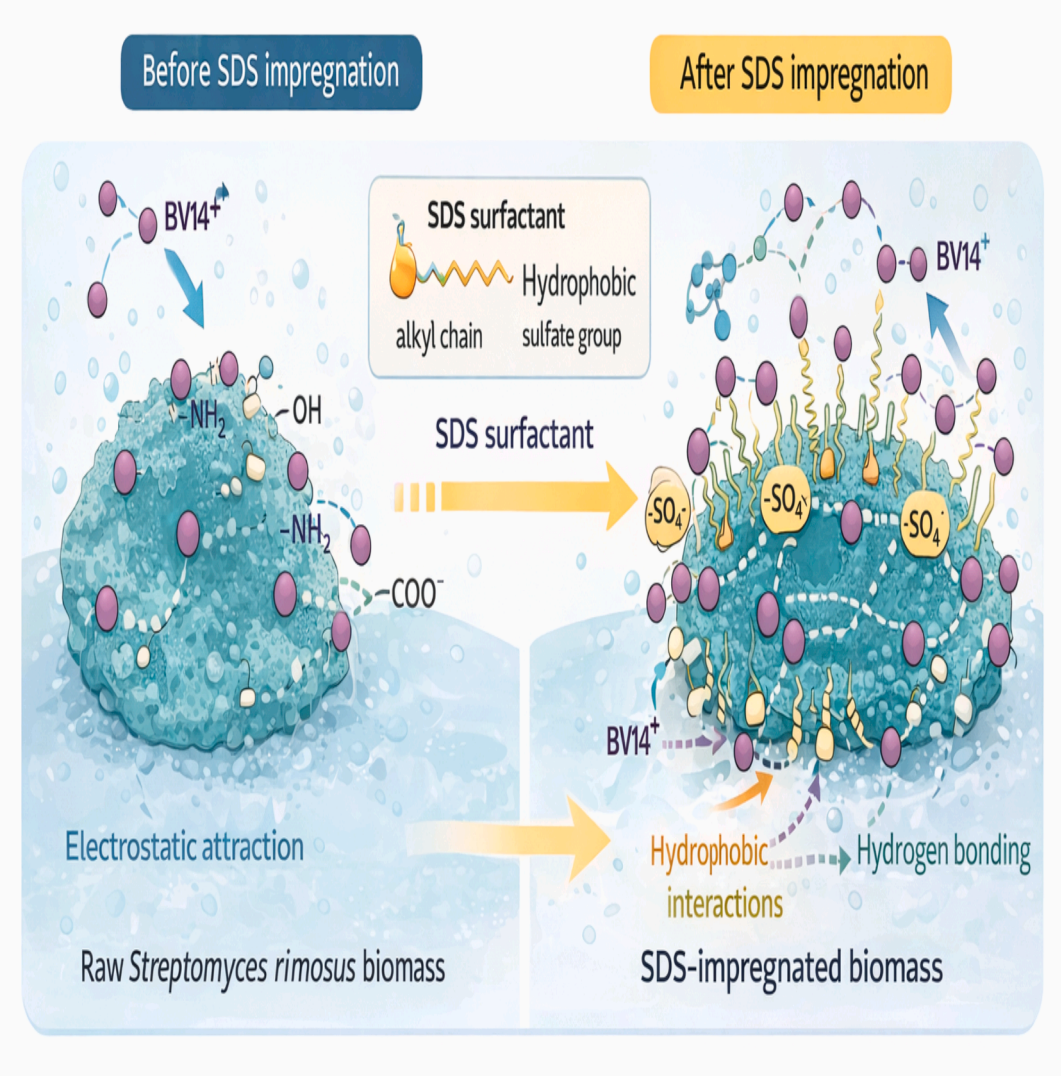

Fig. 2. Proposed adsorption mechanism of BV14 dye onto SR and SDS-SR biomasses.

2.12. Optimization algorithms

In this study, advanced optimization methods were applied, Genetic Algorithm (GA) and Particle Swarm Optimization (PSO). A Genetic Algorithm (GA) is a kind of metaheuristic that is modeled after natural evolution in a population. First, a set of different solutions is proposed, their suitability is assessed, and evolution happens through selection, crossover, and mutation from one generation to the next. It is especially strong at solving complex, multimodal, or discrete search spaces, but to keep its performance high, the parameter tuning (crossover and mutation rates) need to be carefully set to avoid overconvergence or an empty search pool (Katoch et al., 2021).

Particle Swarm Optimization (PSO) is based on the group actions of birds and fish. It contains particles that are defined by both their positions and velocities. Each particle adjusts how it moves using its own best experiences as well as the swarm's global best, helping the group to travel efficiently in nonlinear and continuous spaces. PSO is valued for its simplicity and speed; however, it still requires the development of advanced versions to avoid premature trapping in local optima (Gad, 2022).

3. Results and discussion

3.1. Impregnation process and characterization of adsorbent

Since adsorption is a surface phenomenon, the properties and characterization of the adsorbent surface play a decisive role in its adsorption performance. These analyses aimed to confirm the successful impregnation of SDS onto the SR surface and elucidate the functional groups involved in the adsorption mechanism of the cationic BV14 dye.

A) Fourier-transform infrared (FTIR) spectroscopy was used to identify the main surface functional groups of SR biomass, SDS-modified biomass (SDS-SR), and SDS-SR after BV14 adsorption (Fig. 1. A).

For **SR biomass**, the broad band around 3334–3281 cm^{-1} corresponds to overlapping –OH and –NH stretching vibrations, indicating hydroxyl and amino groups. The band at ~ 1638 cm^{-1} is attributed to C=O stretching (carboxyl or amide groups), while the band close to 1028 cm^{-1} is attributed to C–O stretching of polysaccharides (Kirova et al., 2021). **After SDS impregnation (SDS-SR)** new characteristic peaks appear at 2916 and 2850 cm^{-1}, assigned to alkyl C–H stretching vibrations of the SDS hydrophobic chains. Moreover, different bands are observed at 1216, 994, and 825 cm^{-1} which correspond to $–SO_4^-$ (sulfate) groups confirming successful SDS impregnation and introduction

of anionic functional groups onto the biomass surface (Bat-Amgalan et al., 2021). **After BV14 adsorption**, large spectral changes are detected. The peaks related to sulfates (1216, 994, 825 cm^{-1}) decrease significantly or disappear, indicating the existence of strong electrostatic interactions between the $-SO_4^-$ groups and the cationic dye. The band around 994 cm^{-1} shifts to 1025 cm^{-1}, which suggests changes in the chemical environment of sulfate or polysaccharide groups (Que et al., 2018). Additionally, a slight shift of the C=O band (1638 to 1625 cm^{-1}) indicates possible hydrogen bonding interactions between BV14 molecules and native functional groups of the biomass (Othmani et al., 2025). These results prove that sulfate groups introduced by SDS play the dominant role in BV14 adsorption, with additional contributions from the native hydroxyl and carbonyl groups (Djebbah et al., 2022).

B) X-ray diffraction (XRD) analysis was carried out to assess the structural organization and crystalline variation of the SR biomass before and after SDS impregnation (Zhao et al., 2020). The XRD patterns of SR biomass before and after SDS impregnation show the predominance of amorphous structural features with noticeable modifications after surfactant treatment (Fig. 1. B). **The raw SR biomass** shows a wide diffraction halo centered at $2\theta \approx 20–25°$ typical for amorphous organic materials such as polysaccharides, proteins and other biopolymers, and indicating a lack of long-range crystalline order. **After SDS**

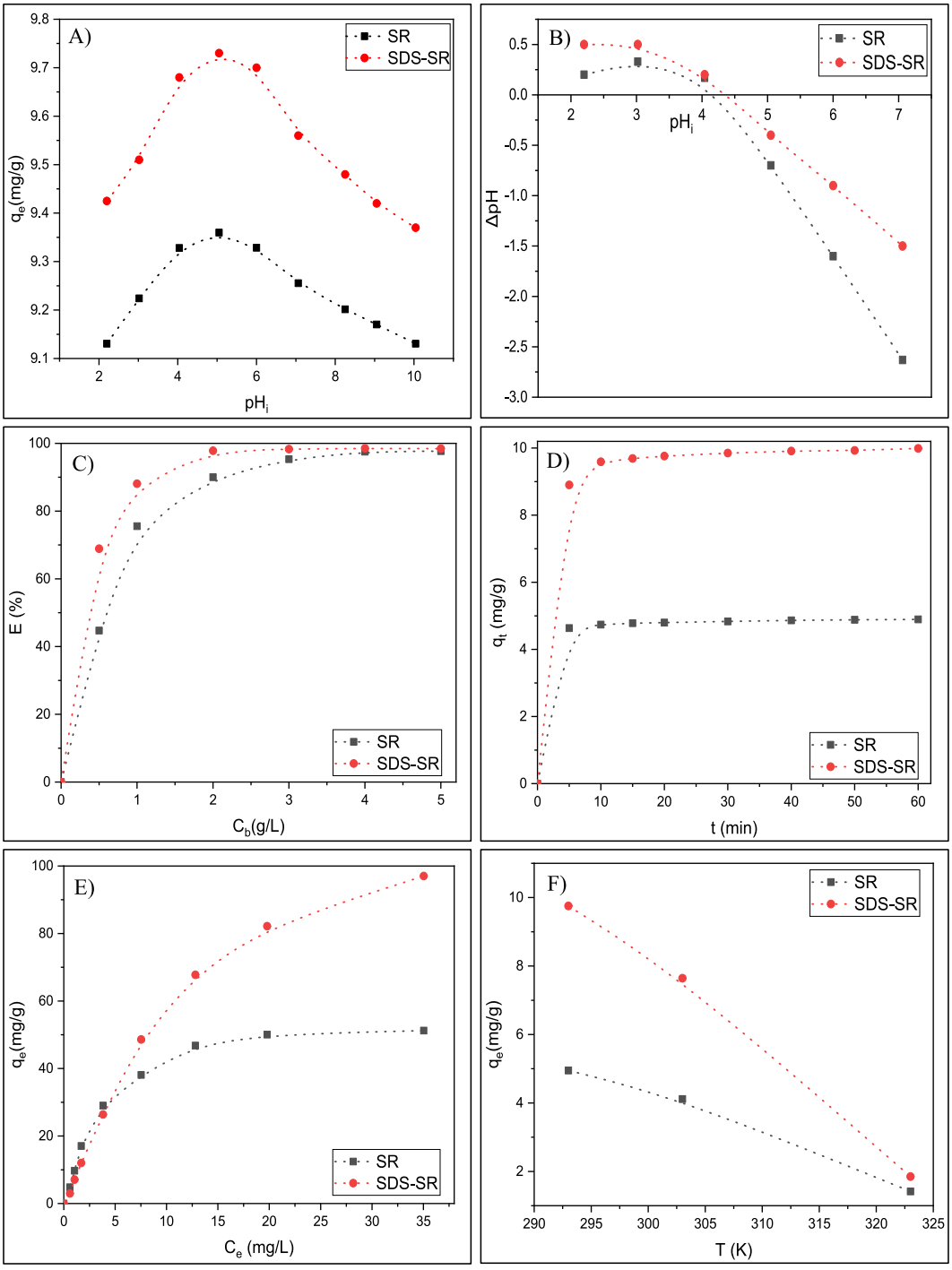

Fig. 3. Effects of A) solution pH, B) point of zero charge pH_{pzc}), C) adsorbent dose, D) contact time, E) initial dye concentration, and F) temperature on the adsorption capacity of BV14 onto SR and SDS-SR biomasses; G) thermodynamic modeling; and H) desorption cycles for BV14 on (a) SR biomass and (b) SDS-SR biomass.

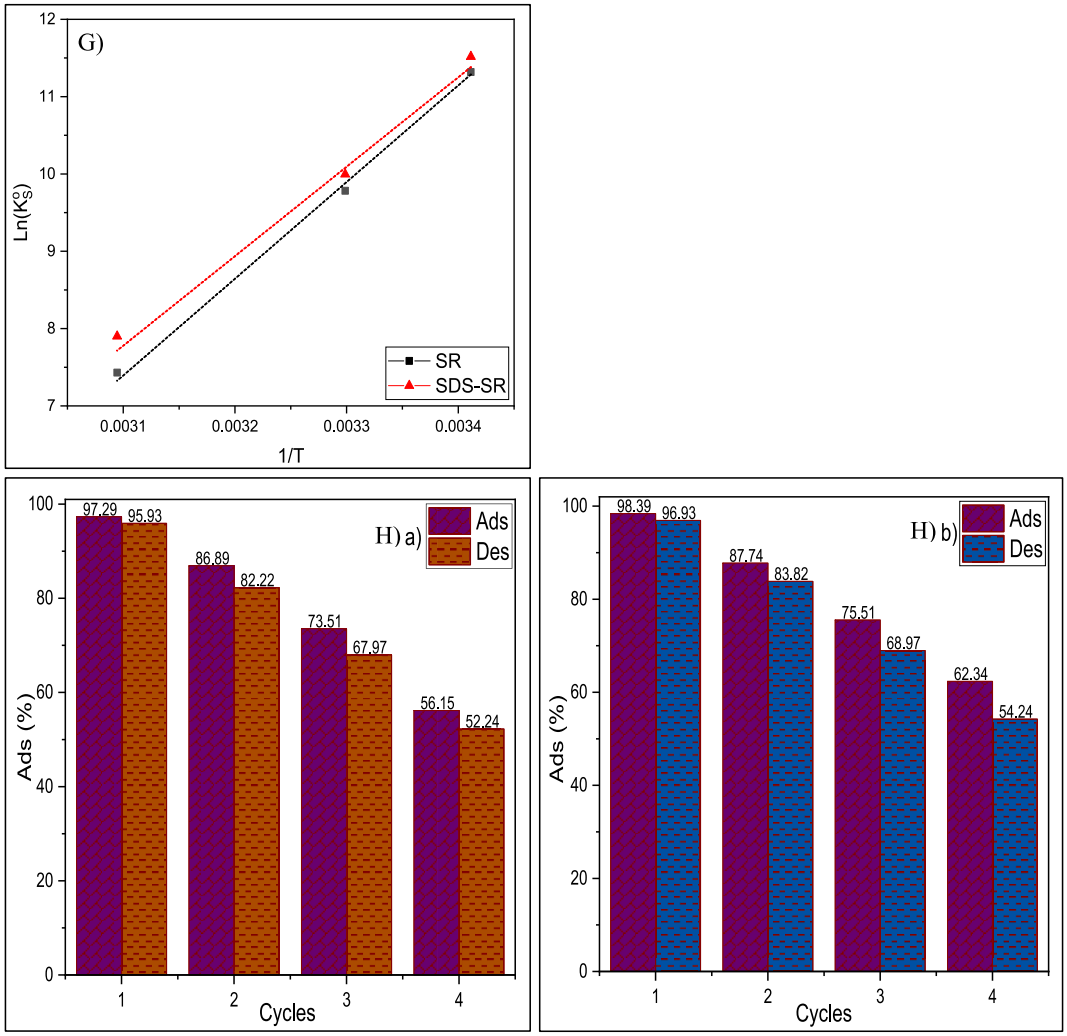

Fig. 3. (*continued*).

impregnation, the overall amorphous profile is preserved, although minor alterations in peak intensity and appearance of weak additional reflections are suggestive of incorporation of SDS molecules on the biomass surface. The increased intensity and slight sharpening in the 20–25° region may be attributed to partial organization of the dodecyl chains and short-range order induced from surfactant self-assembly. No sharp crystalline peaks corresponding to bulk crystalline SDS are observed suggesting that SDS is well-dispersed and mainly adsorbed instead of forming separate crystalline domains. These structural modifications confirm successful impregnation and suggest that SDS adsorption induces surface reorganization without altering the intrinsic amorphous nature of the biomass, thereby preserving its porous structure while introducing functional domains favorable for enhanced dye adsorption (Othmani et al., 2026).

C) X-ray photoelectron spectroscopy (XPS) is a surface-sensitive technique that is used to determine the elemental composition, oxidation states and chemical functionality within the top ~ 5–10 nm of SR and SDS-SR biomasses. It provides both survey spectra (elemental and atomic identification) and high-resolution spectra (chemical state analysis through peak deconvolution). X-ray photoelectron spectroscopy (XPS) revealed significant surface chemical differences between the SR and SDS-SR biomasses, directly correlating with the enhanced adsorption of BV14 dye (Fig. 1. C). **The SR biomass** spectrum is mainly dominated by C1s (~284.8 eV) and O1s (~532 eV) peaks related to C–C/C–H, C–O, C=O, and O–C=O groups of the biopolymeric structures along with a minor contribution of N1s (~400 eV) from amine/amide functionalities. A Na1s signal is also observed in SR which is attributed to an intrinsic sodium in the raw biomass. **After SDS impregnation**, a distinct S2p peak around 169 eV confirms the successful immobilization of dodecyl sulfate anions, and the intensity of Na1s peak is not affected which indicates that the Na^+ from SDS is not retained on the surface. An increase in the C–C/C–H contribution is a further reflection of the incorporation of aliphatic chains. Compared to the raw biomass, whose adsorption capacity relied mainly on native carboxyl groups and hydrogen bonding, the SDS-impregnated material exhibits a dual interaction mechanism toward cationic BV14: strong electrostatic attraction between $-SO_4^-$ groups and the positively charged dye molecules, together with additional hydrophobic interactions between the dye's aromatic structure and the alkyl chains (Xu et al., 2023). This synergic effect increases the dye-surface affinity and stabilizes adsorption, and therefore explains the improved adsorption capacity obtained after SDS impregnation.

D) Thermogravimetric analysis (TGA) was performed to evaluate the thermal stability and decomposition behavior of the SR and SDS-SR biomasses (Fig. 1. D). **The SR biomass** shows a typical multi-step degradation profile, first with a weight loss at low temperature due to the evaporation of moisture followed by a major degradation stage related to the breakdown of organic constituents such as proteins, polysaccharides and lipids (Amiri and Raayatpisheh, 2024). **The SDS-SR biomass** exhibits a modified thermal behavior in terms of slightly shifted main degradation region and higher residual mass at high temperature. The altered decomposition pattern indicates successful

incorporation of SDS onto the biomass surface, where the surfactant contributes additional organic content and modifies the thermal decomposition pathway. The enhanced residual mass and smoother degradation slope imply better thermal stability which is probably attributed to the interactions between the sulfate headgroups and surface functional groups and partial surface coverage by the hydrophobic dodecyl chains (Almas et al., 2023). Overall, the TGA results confirm effective SDS impregnation and demonstrate that the surfactant induces measurable changes in the thermal stability of the biomass without disrupting its fundamental decomposition profile.

Table 1
Kinetic model parameters, isotherm model parameters with error analysis, and thermodynamic parameters for the adsorption process.

Section	Model	Parameter	SR			SDS-SR		
Kinetics	Pseudo-first order	q_e (mg/g)	4.89			9.99		
		q_1 (mg/g)	4.830			9.837		
		k_1 (min^{-1})	0.633			0.463		
		R^2	0.999			0.998		
		MSE	0.002			0.009		
		RMSE	0.044			0.098		
	Pseudo-second order	q_e (mg/g)	4.89			9.99		
		q_2 (mg/g)	4.894			10.083		
		k_2 (mg/g·min)	0.682			0.157		
		R^2	0.999			0.999		
		MSE	0.001			0.002		
		RMSE	0.016			0.042		
Isotherms	Experimental	q_{max} (mg/g)	51.242			97.015		
Two-parameter Isotherms	Langmuir	q_{max} (mg/g)	60.102			141.430		
		K_L	0.229			0.067		
		R^2	0.994			0.996		
		MSE	2.203			4.110		
		RMSE	1.484			2.027		
	Freundlich	K_F	15.315			13.506		
		n	2.645			1.731		
		R^2	0.924			0.967		
		MSE	27.302			40.050		
		RMSE	5.225			6.328		
	Jovanovic-monolayer	q_{max}	50.586			103.195		
		K_J	0.209			0.0811		
		R^2	0.996			0.9981		
		MSE	1.242			1.262		
		RMSE	1.114			1.123		
Three-parameter Isotherms	Jovanovic-multilayer	q_{max}	47.680			120.707		
		K_J	0.230			0.068		
		KK_J	0.0021			−0.003		
		R^2	0.9972			0.9983		
		MSE	1.035			1.154		
		RMSE	1.017			1.074		
	Hill	q_{max}	54.966			117.355		
		K_H	4.718			17.734		
		n_H	1.239			1.248		
		R^2	0.998			0.999		
		MSE	0.723			0.132		
		RMSE	0.850			0.363		
	Redlich-Peterson	a_{RP}	11.270			7.686		
		β_{RP}	0.114			0.015		
		K_{RP}	1.144			1.346		
		R^2	0.9978			0.9988		
		MSE	0.813			0.785		
		RMSE	0.902			0.886		
	Sips	q_S (mg/g)	54.966			100.656		
		k_S (min^{-1})	0.286			0.363		
		n_S	1.239			1.307		
		R^2	0.998			0.999		
		MSE	0.723			0.132		
		RMSE	0.850			0.363		
	Toth	q_T (mg/g)	117.117			1353.264		
		k_T (min^{-1})	8.466			63.429		
		n_T	1.087			1.2421		
		R^2	0.9975			0.9986		
		MSE	0.825			0.893		
		RMSE	0.908			0.945		
Thermodynamics		T (K)	297	307	327	297	307	327
		K_S (L/mg)	0.286	0.043	0.005	0.363	0.042	0.008
		$K°_S$	9.6E4	1.4E4	1689	1.2E5	1.4E4	2702.4
		$Ln(K°_S)$	11.478	9.584,	7.432	11.717	9.560	7.902
		$\Delta G°$ (kJ/mol)	−27.97	−24.15	−19.97	−28.55	−24.09	−21.23
		$\Delta H°$ (kJ/mol)	−96.208,			−103.983,		
		$\Delta S°$ (J/mol·K)	–233.557,			−260.869,		

E) Brunauer–Emmett–Teller (BET) analysis was performed using N_2 adsorption–desorption measurements to assess the changes of the specific surface area of the SR biomass before and after SDS impregnation (Fig. 1. E) **The SR biomass** exhibited a relatively low BET surface area of 3.2 m^2/g, reflecting its limited accessible porosity and compact biopolymeric structure. **After SDS impregnation**, the surface area highly increased to 8.81 m^2/g which enhances the accessibility of the adsorption site. The corresponding isotherm of SDS-SR reveals a higher adsorption volume in the measured range of relative pressure in comparison to SR and confirms the enhanced nitrogen uptake. This increase can be attributed to surface restructuring induced by SDS molecules in which electrostatic anchoring of sulfate groups and outwards orientation of dodecyl chains is likely promoting partial dispersion of biomass aggregates and improved pore accessibility (Que et al., 2018). Additionally, the surfactant layer may generate new interfacial voids and prevent pore collapse, contributing to the observed increase in surface area. Overall, the BET results demonstrate that impregnation with SDS is effective in improving the textural properties of biomass, offering a larger accessible surface supporting the improved adsorption performance towards dye molecules.

F) Scanning electron microscopy (SEM) was performed to investigate the surface morphology of SR biomass at 800 × magnifications before and after BV14 adsorption (Fig. 1. F). **The SR biomass** exhibits a heterogeneous and rough surface with irregular fragments and visible voids, indicating a porous structure ranging in diameter size from 18.23 to 27.10 µm favorable for adsorption (Sorour et al., 2023). **After BV14 adsorption**, the surface appears more compact and partially covered by deposited layers, accompanied by reduced pore visibility and smoother regions. These morphological changes confirm that dye is attached onto the surface of biomass which could be attributed to electro-statistical and hydrophobic interactions, which result in surface coverage and partial filling of accessible pores; this supports the proposed adsorption mechanism which involves surface binding and accumulation of dye molecules (Jaymand, 2024).

Adsorption mechanism

The adsorption of Fuchsin dye (Basic Violet 14, BV14) onto *Streptomyces rimosus* biomass occurs through a combination of electrostatic interactions, hydrogen bonding, and van der Waals forces, largely governed by the functional groups present on the biomass surface (Fig. 2).

In the raw biomass, adsorption is mainly driven by functional groups present on the surface such as carbonyl (C=O), carboxyl (–COOH), hydroxyl (–OH), and amine ($–NH_2$). These groups interact with the cationic Fuchsin dye molecules through electrostatic attraction, particularly under acidic conditions where the biomass surface becomes negatively charged. However, the density and accessibility of these active sites are limited, which constrains the overall adsorption capacity (Bouchelkia et al., 2025).

Upon impregnation with sodium dodecyl sulfate (SDS), the biosorbent surface undergoes significant physicochemical enhancement. SDS, an anionic surfactant, introduces negatively charged sulfate groups ($–SO_4^-$) onto the biomass surface. These groups increase the net negative surface charge, thereby intensifying the electrostatic attractions between the biosorbent and the positively charged dye molecules. This modification also improves surface wettability, pore accessibility, and the overall number of active binding sites available for dye adsorption (Alamin et al., 2021).

As a result, the SDS-impregnated biomass exhibits a much higher adsorption capacity and faster binding kinetics compared to the raw biomass. The combination of enhanced surface charge and increased functional site density leads to stronger and more numerous interactions with Fuchsin molecules (Grigoraș et al., 2022).

3.2. Batch adsorption study

This paper investigated, in a batch mode, the effect of several parameters including initial pH (pH_i), adsorbent dose (C_b), contact time (t), initial concentration (C_i) and temperature (T) on the adsorption performance of two biomasses: raw biomass (SR) and impregnated biomass with a surfactant (SDS-SR).

3.3. Effect of initial pH

As part of a comparative study of the effect of initial pH (pH_i) on the adsorption capacity of once SR biomass and another SDS-SR biomass, the pH_i of a solution with an initial dye concentration of $C_i = 20$ mg/L and volume V = 50 mL was varied from 2 to 10 by adding a solution of 0.1 N HCl or 0.1 N NaOH, then brought into contact with the biomass, $C_b = 2$ g/L (SR or SDS-SR), the temperature of the solution was kept constant at 297 K for contact time of 120 min.

Fig. 3. A demonstrates that the maximum adsorption capacity of BV14 occurs in the acidic pH range (below pH 7), particularly between pH 4 and 6. In this range, the biomass surface is negatively charged for both raw SR and SDS-SR, highlighting the role of electrostatic attraction between the negatively charged adsorbent surface and the cationic dye molecules, which becomes favorable above the pH_{PZC} (4.3–4.5) (Azoulay et al., 2023). The maximum adsorption capacities of 9.3 mg/g for SR and 9.7 mg/g for SDS-SR were observed at pH 5, confirming clearly that BV14 adsorption is strongly favored under acidic conditions, primarily due to electrostatic interactions (Ali et al., 2022).

The points of zero charge (pH_{PZC}) of SR and SDS-SR were determined as 4.3 and 4.5, respectively (Fig. 3.B). According to zero-charge point theory, when $pH < pH_{PZC}$, the surface becomes positively charged, favoring anion adsorption, and when $pH > pH_{PZC}$, the surface becomes negatively charged, favoring cation adsorption, indicating a shift in electrostatic behavior that influences dye interaction (Al-Maliky et al., 2021).

However, although the surface becomes more negatively charged at higher pH (6–10), the adsorption capacity decreases. This is mainly due to the increased concentration of OH^- ions, which compete with the cationic BV14 molecules for active sites and partially screen electrostatic interactions. In addition, alkaline conditions may alter dye speciation or promote aggregation, reducing its effective interaction with the adsorbent. Therefore, optimal adsorption occurs around pH 5, where electrostatic attraction and dye stability are balanced (Sassi et al., 2023).

3.4. Effect of adsorbent dose

The effect of adsorbent dose on the removal of BV14 by once *SR* and another SDS-*SR* biomass was investigated by varying it from 0.5 to 5 g/L while keeping the solution volume constant at V = 50 mL, $C_i = 20$ mg/L, $pH_i = 5$ at 297 K. The results are presented in Fig. 3.C.

BV14 removal efficiency increased by increasing adsorbent dose, reaching a plateau at 4 g/L for SR and 2 g/L for SDS-SR (Fig. 3.C). Removal efficiencies for both adsorbents increased from 44% to 97% (SR) and from 68% to 98% (SDS-SR) when the adsorbent dose was increased from 0.5 to 5 g/L. Above 4 g/L for SR and 2 g/L for SDS-SR, removal efficiency became stable. This initial increase is attributed to the high availability of adsorption sites and the expansion of the effective surface area. However, as the adsorbent dose increases, adsorption sites become progressively saturated and intermolecular interactions between adsorbent particles intensify, leading to solid aggregation (Bouchelkia et al., 2023b). This results in a decrease in removal efficiency (E) and adsorption capacity (q_e).

Therefore, an adsorbent dose of 4 g/L for *SR* and 2 g/L for SDS-*SR* was considered optimal for the removal of BV14 dye. Under these respective conditions the maximum adsorption capacity (q_{max}) was 4.89 mg/g for SR at 4 g/L whereas SDS-SR was 9.99 mg/g at only 2 g/L, showing a nearly twofold increase in adsorption capacity. These results clearly indicate that SDS-SR can assure the same removal percentage as SR while requiring only half dosage of biosorbents. Consequently, all subsequent adsorption experiments were carried out at these optimized doses.

3.5. Effect of contact time

To evaluate whether the impregnation of biomass influences its adsorption rapidity, we tested the contact time for both *SR* and SDS-*SR*. (Fig. 3.D) shows contact time effect on the amount of adsorption (q_t) of BV14 by *SR* and SDS-*SR* at a constant solution volume V = 50 mL, C_i = 20 mg/L, pH_i = 5, C_b = 4 g/L for SR and 2 g/L for SDS-SR and at a constant temperature of 297 K.

Adsorption amount of BV14 by both SR and SDS-SR increased with time, with a notable rise observed between 2 and 30 min in both adsorption amount and removal percentage of BV14. This significant increase during the initial phase is attributed to the abundant availability of active adsorption sites, which later stabilizes as the system reaches equilibrium (Bouchelkia et al., 2023a). BV14 removal is instantaneous. At 30 min, the adsorption capacities of SR and SDS-SR were approximately 4.8 mg/g and 9.8 mg/g, respectively. After 60 min, these values slightly increased to 4.9 mg/g and 9.9 mg/g, indicating that adsorption equilibrium was effectively reached within this period, with no significant change observed at longer contact times. This indicates that the equilibrium was achieved within 60 min, and subsequent experiments were carried out using a contact time of 60 min.

3.6. Effect of initial concentration

In a continuation of the comparative study between the adsorption capacity of the SR with 4 g/L dose and SDS-SR with 2 g/L dose, for an optimal contact time t = 60 min, pH_i = 5 and at a constant temperature of 297 K, the effect of varying the initial concentration of BV14 C_i from (10–250 mg/L) on adsorption was investigated, as shown in Fig. 3.E.

The adsorption capacity of both SR and SDS-SR increased with increasing initial concentrations from 10 to 250 mg/L. When the initial concentration is increased from (10–250 mg/L), the adsorption capacity increases to reach 51 mg/g for SR and from 97 mg/g for SDS-SR.

As the initial concentration of BV14 increases, the adsorption capacity (q_e) of the biosorbent also increases, eventually reaching a plateau. This behavior is attributed to the finite number of active sites available on the adsorbent surface, which become progressively saturated as the dye concentration rises (Cheikh et al., 2023). At higher concentrations, the driving force for mass transfer is greater, reducing resistance to adsorption and enhancing the rate at which dye molecules migrate to the biosorbent surface (Aminu et al., 2020). However, once all active sites are occupied, further increases in dye concentration do not lead to a corresponding increase in adsorption capacity.

Table 2
Quantum chemical descriptors (HOMO–LUMO, μ, η, S, ω, N) and computed adsorption energies.

Section	Molecule / System	Parameter	Value
Quantum Chemical Descriptors	BV14	E_T (a.u.)	−938.344
		E_{HOMO} (eV)	−5.4879
		E_{LUMO} (eV)	−2.8895
		μ (Debye)	12.8722
		μ (eV)	−4.1887
		η (eV)	2.5984
		S (eV)	0.3848
		ω (eV)	3.376
		N (eV)	1.744
	SDS	E_T (a.u.)	−1171.695
		E_{HOMO} (eV)	−7.4622
		E_{LUMO} (eV)	0.2076
		μ (Debye)	36.1028
		μ (eV)	−3.6272
		η (eV)	7.6698
		S (eV)	0.1303
		ω (eV)	0.857
		N (eV)	−0.230
	LTA	E_T (a.u.)	−2146.440
		E_{HOMO} (eV)	−4.8363
		E_{LUMO} (eV)	−0.1502
		μ (Debye)	22.0802
		μ (eV)	−2.493
		η (eV)	4.6861
		S (eV)	0.2134
		ω (eV)	0.663
		N (eV)	2.3957
Adsorption Energies	BV14 – LTA (SR)	E_{ads} (eV)	−1.42
		Charge transfer (e^-)	0.08
		Adsorption type	Hydrogen bonding + electrostatic attraction
	BV14 – LTA + SDS (SDS-SR)	E_{ads} (eV)	−2.87
		Charge transfer (e^-)	0.21
		Adsorption type	Strong electrostatic binding, π–π, hydrophobic stabilization

3.7. Kinetic of adsorption

Table 1 presents the kinetic parameters derived from the pseudo-first-order and pseudo-second-order models. The correlation coefficients (R^2) obtained from the pseudo-second-order model analysis were found to be significantly close to unity for both biomasses, and the calculated equilibrium adsorption capacities ($q_{e,cal}$) were very similar to the experimentally determined values ($q_{e,exp}$).

These results indicate that adsorption of the BV14 by both biomasses is best described by the pseudo-second-order kinetic model. This model is generally applied to adsorption processes that occur between low-molecular-weight solutes at low concentrations interacting with fine adsorbent particles (Bouchelkia et al., 2023a).

It assumes that chemisorption is the rate-limiting step of adsorption, involving valence forces through electron sharing or exchange between the adsorbate and the adsorbent (Jasri et al., 2023).

3.8. Isotherm of adsorption

Based on the lowest values of the error functions (MSE and RMSE) and the highest correlation coefficients (R^2), the adsorption data for both SR and SDS-SR biomasses were best described by the Hill and Sips isotherm models (Table 1).

The models ranked in the following order of fit quality: Hill = Sips > Redlich–Peterson > Toth > Jovanovic (Multilayer) > Jovanovic (Monolayer) > Langmuir > Freundlich. This hierarchy provides important information about BV14 adsorption, which confirms surface heterogeneity effects with cooperative binding and the potential development of multiple layers.

The high performance of Hill model, the absorption at one site reinforces similar absorption at adjacent sites (J. Li et al., 2024), while Sips model suggests that adsorption occurs through heterogeneous binding and attains saturation at high concentrations (Obayomi et al., 2023).

The relatively good fit of Redlich-Peterson (Ismail et al., 2025) and Toth models (Mabuza and Mahlobo, 2025) confirms the occurrence of non-ideal adsorption, while Toth model is particularly well suited to describe deviations from linearity at high solute-ion concentrations.

The better performance of Jovanovic (Nandiyanto et al., 2024) multilayer model compared to its monolayer suggests the possible formation of multiple adsorption layers that classical models cannot explain.

In contrast, the weaker fits of both Langmuir and Freundlich models imply that the hypotheses about surface homogeneity and purely empirical monolayer adsorption are unsuitable for this system (Sahnoun et al., 2024).

Collectively, these results suggest a complex adsorption mechanism involving heterogeneous binding sites, cooperative adsorption behavior, and potential multilayer development (Hamri et al., 2024).

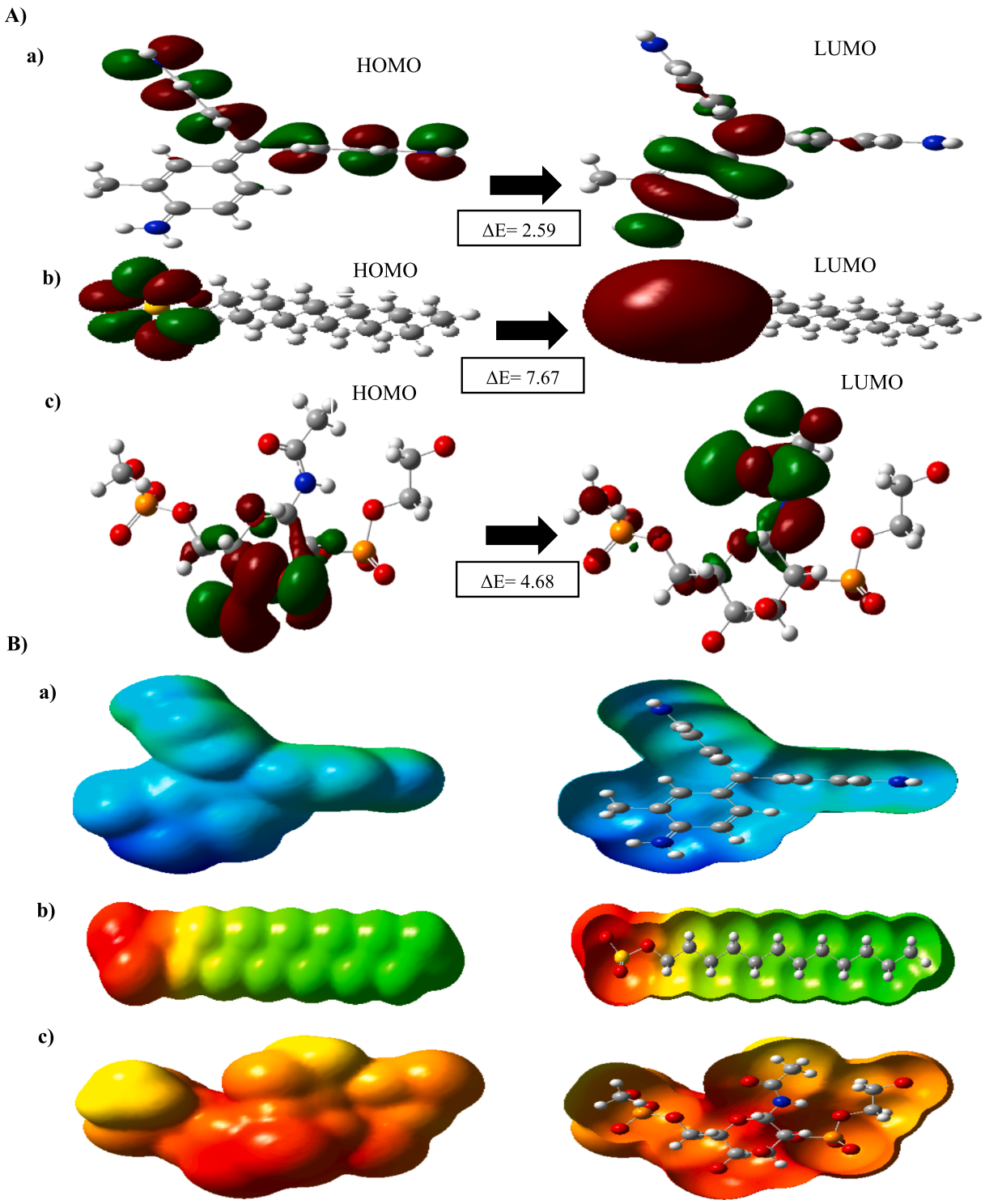

Fig. 4. A) HOMO–LUMO orbital distribution and B) molecular electrostatic potential (MEP) maps of a) BV14, b) SDS, and c) LTA, illustrating the electronic structure and electrostatic complementarity between the cationic regions of the dye and the anionic sulfate/phosphate groups of the surface models.

3.9. Thermodynamics of adsorption

To conduct a more comprehensive comparative study of the adsorption capacities of the two biomasses, $C_b = 4$ g/L of SR and $C_b = 2$ g/L of SDS-SR were brought into contact with V = 50 mL of dye solution at an initial concentration of $C_i = 20$ mg/L. The experiments were carried out at the optimum contact time of 60 min and an initial pH of $pH_i = 5$, under various temperatures (297 K, 302 K, 327 K), as illustrated in Fig. 3.F.

It is observed that adsorption of BV14 decreases as the temperature rises, which indicate that higher temperatures significantly reduce the adsorption capacity of both SR and SDS-SR, it can increase kinetic energy of BV14 molecules, causing adsorbates to desorb from adsorbent surface (Ebelegi et al., 2020). It can also provide enough potential

Table 3
Comparative interpretation of experimental adsorption trends in relation to dft results.

Observation	Experimental Result	DFT Interpretation
Higher q_{max} for SDS-SR	97 mg/g vs 51 mg/g	Larger
More negative ΔH° for SDS-SR	−103.98 vs − 96.21 kJ/mol	Stronger binding & charge transfer
Faster equilibrium contact time	30–60 min	Lower HOMO–LUMO gap → higher reactivity
Hill/Sips isotherm best fit	Cooperative + heterogeneous adsorption	Multiple interaction sites confirmed
Pseudo-second-order kinetics	Chemisorption-influenced process	Charge redistribution & H-bonding visible in Mulliken and geometry

Table 4
Statistical performance indicators (R, R^2, and RMSE) for the tested models applied to SR and SDS-SR biomasses, and optimization results obtained using genetic algorithm (GA) and particle swarm optimization (PSO) coupled with the ANN model.

Model	Parameter	SR	SDS-SR
ANN	R^2 (Train)	1.0000	0.9995
	R^2 (Test)	0.9951	0.9960
	R^2 (All)	0.9977	0.9985
	RMSE (Train)	0.0051	0.8355
	RMSE (Test)	3.0856	4.3492
	RMSE (All)	1.0146	1.5032
Linear Regression	R^2 (Train)	0.9744	0.9867
	R^2 (Test)	0.9747	0.9860
	R^2 (All)	0.9745	0.9869
	RMSE (Train)	3.1548	4.6141
	RMSE (Test)	1.4029	1.1838
	RMSE (All)	3.0149	4.4255
Decision Tree	R^2 (Train)	0.9651	0.9798
	R^2 (Test)	0.9591	0.9360
	R^2 (All)	0.9627	0.9790
	RMSE (Train)	3.2767	5.6495
	RMSE (Test)	5.8950	5.1058
	RMSE (All)	3.6514	5.6050
Random Forest	R^2 (Train)	0.9507	0.9447
	R^2 (Test)	0.9760	0.5113
	R^2 (All)	0.9513	0.9722
	RMSE (Train)	7.4208	15.0586
	RMSE (Test)	3.2109	4.3187
	RMSE (All)	7.0873	14.4542
ANN-GA Optimization	GA Optimal Conditions	$X_1 = 60.00$, $X_2 = 1.31$, $X_3 = 240.10$, $X_4 = 5.08$, $X_5 = 20.85$	$X_1 = 60.00$, $X_2 = 1.91$, $X_3 = 239.02$, $X_4 = 5.09$, $X_5 = 23.98$
	GA Max Adsorption (mg/g)	56.09	99.30
ANN-PSO Optimization	PSO Optimal Conditions	$X_1 = 60.00$, $X_2 = 1.28$, $X_3 = 240.00$, $X_4 = 5.10$, $X_5 = 20.00$	$X_1 = 60.00$, $X_2 = 1.90$, $X_3 = 239.00$, $X_4 = 5.10$, $X_5 = 24.00$
	PSO Max Adsorption (mg/g)	56.08	99.56

energy which results in weakening bounds of BV14 molecules from the biomass surface (Shefer et al., 2022). It can also change the biomass surface properties, reducing its affinity and porosity for the dye (Supriya et al., 2022).

K_S^0 is the dimensionless thermodynamic Sips constant that describes the adsorption process. K_s is derived from the isotherm Sips constant (5), K_s in (L/mg) was converted to a molar basis and normalizing it using a standard state concentration of $C^0 = 1$ mol/L according to the following equation (Benazouz et al., 2025):

$$KS0 = Ks\left(\frac{L}{mg}\right).1000\left(\frac{mg}{g}\right).MBV14\left(\frac{g}{moL}\right).C0\left(\frac{moL}{L}\right) \quad (5)$$

$M_{BV14} = 63.546$ g/mol, is the molar mass of BV14, and the 1000 factor is used to convert milligrams to grams.

The enthalpy changes ΔH, and the entropy change ΔS, were determined from the slope and intercept of the plot of Ln (K_S°) versus 1/T (Fig. 3.G) and presented in Table 1.

Thermodynamic analysis of BV14 adsorption on SR and SDS-SR biomasses shows that the process occurs spontaneously at lower temperatures through negative values of the Gibbs free energy change (ΔG°). However, the increasing values of ΔG° as temperature rises, suggest that the adsorption spontaneity decrease where higher temperatures can hinder adsorption due to increased molecular motion. Both biomasses exhibited negative enthalpy changes during adsorption (ΔH°) which demonstrated the exothermic nature of dye removal while SDS-SR showed greater exothermic behavior (−103.983 kJ/mol) than SR (−96.208 kJ/mol) because of its multiple enhanced dye–adsorbent interaction, such as electrostatic attraction, ion exchange or even strong hydrogen bonding.Although the process is largely driven by physical adsorption mechanisms, the ΔH° value exceeding − 40 kJ/mol indicates possible contributions from stronger interactions such as ion-exchange or partial chemisorption contribution (Calisto et al., 2019). Additionally, the negative entropy change (ΔS°) values of both systems reveal a reduction of solid–liquid interface randomness, yet SDS-SR again exhibits a more pronounced disorder decrease (−260.869 J/mol/k). The results of BV14 adsorption onto both biomasses primarily occurs through spontaneous and exothermic mechanisms that reduce entropy while SDS modification enhances adsorption performance, increasing affinity, spontaneity, and heat release (Hamri et al., 2025).

3.10. Desorption study

Desorption studies focus mainly on evaluating adsorbent reuse and issues of sludge disposal. The ability of an adsorbent to maintain its performance over several adsorption–desorption cycles is essential for its practical and economical use. Since wastewater treatment is costly, adsorbent regeneration is essential for economic viability. Limited reusability or significant efficiency loss increases operational costs and may contribute to secondary environmental contamination (Sandollah et al., 2020).

The removal efficiency of BV14 dye by both SR and SDS-SR progressively decreased from 97.29 to 56.15% and from 98.3 to 62.34% respectively over four adsorption–desorption cycles (Fig. 3.H). The slight decrease in adsorption efficiency observed after successive regeneration cycles, can be attributed to several physicochemical factors. First, the repeated exposure to the stripping agent and agitation can induce minor surface modifications with a slight effect on the accessibility and distribution of active sites (Goldberg et al., 2007). Although the overall structure remains stable, minor mass loss during washing steps may contribute to the gradual decline in performance.

Second, partial pore blockage caused by incomplete desorption of strongly bound BV14 molecules may further reduce the number of the available active sites in the succeeding cycles. Residual dye species retained within microporous or heterogeneous regions can progressively limit adsorption efficiency. In addition, the ion-exchange mechanism involved in the adsorption of BV14 may not be fully reversible. The negatively charged sulfate ($-SO_4^-$) groups introduced by SDS are involved in electrostatic attraction and ion exchange with cationic BV14 molecules and repeated cycles may result in a gradual reduction in accessibility of these exchangeable sites. Competitive replacement by protons or other ions from the stripping solution may not completely restore the original surface configuration (Zhang et al., 2024).

Third, minor surfactant leaching from the SDS modified biomass may be experienced during regeneration process. Since the enhanced adsorption performance of SDS-SR is contributed by the existence of sulfate-rich functional groups introduced by SDS, even limited surfactant loss may reduce electrostatic attraction and hydrophobic interactions between the biosorbent and BV14 molecules (Guo et al., 2024).

Despite this moderate decline, the biosorbent maintains high removal efficiency over multiple cycles, demonstrating strong stability and regeneration potential. From an economic perspective, its sustained performance reduces material replacement cost and supports cost-effective large-scale wastewater treatment.

3.11. Density functional theory (DFT) results

The global descriptors (Table 2) indicate that BV14 is electronically soft ($\Delta E = 2.59$ eV, $S = 0.385$) and a strong electrophile ($\omega = 3.38$ eV), whereas LTA and SDS fragments are relatively harder ($\Delta E \approx 4.69$ and 7.67 eV, respectively). The chemical potential ordering LTA (−2.49 eV) > SDS (−3.63 eV) > BV14 (−4.19 eV) gives a general tendency of electron flow towards BV14, and this is actually realized by an increase of Mulliken charge redistribution upon the adsorption. SDS in addition exhibits a very large dipole moment and as demonstrated by the Parr indices highly nucleophilic sulfate oxygens; this combination of effects is responsible for the larger electron transfer (≈ 0.21 e^-), and the much more negative adsorption energy for BV14 on SDS-LTA (−2.87 eV) compared to BV14 on unmodified LTA (−1.42 eV). In short, BV14 has a small gap and high electrophilicity, which makes the interactions favorable by charge transfer, and SDS increases electrostatic and donor–acceptor components of binding, which gives a consistent explanation of the enhanced experimental q_{max} and more exothermic adsorption observed for SDS-SR at the quantum level.

The HOMO orbital is mainly delocalized over the aromatic rings and amine groups of BV14, while the LUMO is localized on central conjugated carbons, which confirmed the participation of π electrons and nitrogen atoms in surface binding. This spatial distributions of HOMO and LUMO orbitals (Fig. 4.A) could demonstrate preferable electronic overlap with SDS than lipoteichoic acid sites.

Blue regions are the electropositive domains and red regions are the most electronegative. The strong electronegative zones on the sulfate headgroup of SDS and the phosphate/oxygen groups of LTA are potential interaction sites with the cationic moieties of BV14. As can be seen in the MEP maps (Fig. 4.B) protonated amine groups of BV14 are associated with the most electropositive regions which preferentially interact with highly nucleophilic sulfate oxygens of SDS and phosphate heads of LTA, validating the electrostatic nature of binding.

The Parr function analysis reveals a striking difference in local reactivity of the raw LTA surface and the SDS modified system (Table S3). In the native LTA model, the most nucleophilic positions are the phosphate and carboxylate oxygens ($P^- \sim 0.40$–0.45), which is why a moderate adsorption energy is calculated for BV14 on the unmodified biomass (=-1.42 eV). After the inclusion of SDS, however, the sulfate oxygen atoms display much higher nucleophilic indices (P^- up to 1.03), indicating a much stronger electron-donor capacity towards the cationic BV14 dye. This local nucleophilicity increase is directly proportional to the increase in Mulliken charge transfer (0.21 e- vs 0.08 e-) and the almost two times increase in adsorption energy (−2.87 vs −1.42 eV).

These results show that SDS cannot simply increase the surface charge density, but introduces new high reactivity binding sites which support stronger electrostatic and charge transfer interactions. This quantum-level evidence is consistent with the experimentally determined increase in adsorption capacity (from 97 to 51 mg/g), increase in exothermicity, and increase in sorption kinetics for SDS-SR.

The calculated adsorption energies (Table 2) show that the most negative E_{ads} values are found for BV14 with SDS-SR, followed by BV14 with SR, indicating more (partially chemisorptive) binding in these cases.

Altogether, global and local electronic descriptors, MEP visualization and adsorption energy information furnish a molecular-level rational explanation of the experimentally observed preferential adsorption sequence of BV14 toward SDS-SR than BV14 toward SR biomass.

DFT analysis confirms that BV14 adsorption on SDS modified biomass is thermodynamically more favorable, electronically stronger and structurally more stabilized than on raw SR biomass. The higher adsorption energy, higher charge transfer and multi-interaction binding mode give a molecular level explanation for the improved adsorption capacity, lower equilibrium time, and more exothermic thermodynamic behavior, observed experimentally.

3.11.1. DFT calculations with experimental interpretation

The computational results are fully consistent with the adsorption trends obtained experimentally (Table 2):

These results show that the SDS impregnation improves the dye affinity by increasing the surface charge density and by introducing additional hydrophobic and π–π interactions, which explain the experimentally determined 2X increase in biosorption capacity (Table 3).

3.12. Machine learning modeling and performance analysis

The prediction accuracy of four machine-learning methods (Artificial Neural Network, Linear Regression, Decision Tree and Random Forest) for the adsorption capacity of SR and SDS-SR biomasses for Fuchsin dye was reviewed (Benazouz et al., 2023). In order to measure performance, the model used the correlation coefficient (R), the coefficient of determination (R^2) and the Root Mean Squared Error (RMSE) for both the training and testing data as well as all the data sets. All the results are summarized in Table 4.

ANN, compared to the other machine learning methods, provided the most reliable predictions for both SR and SDS-SR biomass, with R and R^2 approaching 1 and very low RMSE (1.0146 mg/g for SR, 1.5032 mg/g

for SDS-SR). These results prove that the ANN is capable of learning and generalizing complex, nonlinear adsorption patterns, which is most likely because of its multi-layer structure and the way it handles parameter interactions (Madhuranthakam et al., 2024).

Even though Linear Regression successfully predicted the SR and SDS-SR data (R_all = 0.9745, R^2_all = 0.9496 and RMSE_all = 3.0149 mg/g for SR), its reliability decreased in parts of the results displaying non-linear adsorption behavior (mainly at stronger initial dye concentrations or longer contact times), highlighting its limited prediction ability for complex and non-linear systems.

Results revealed that both methods, Random Forest and Decision Tree, displayed contracting performances. The decision tree showed a moderate ability to capture non-linear adsorption patterns. It provided strong results for SR biomass (R_all = 0.9627, R^2_all = 0.9268, RMSE_all = 3.6514 mg/g) and modest outcomes for SDS-SR biomass (R = 0.9790, R^2_all = 0.9584, RMSE_all = 5.6050 mg/g).

On the other hand, the Random Forest model did not perform well when predicting both biomasses. For SR, even though an R_all of 0.9513 and R^2_all of 0.9049 were reached, yet the model was yielding to higher RMSE_all = 7.0873 mg/g. For SDS-SR, the model produced the poorest results among all, with RMSE_all = 14.4542 mg/g. These results suggest that Random Forest failed to capture the complex interactions introduced by SDS modification and may have suffered from instability in feature learning.

Overall, ANN provided the best results, followed by Linear Regression, Decision Tree and then Random Forest. The results of the ANN model were further validated by the graphical analysis shown in Figs. S2 A, B and C.

Fig. S2.A compared experimental data against the ANN predicted values of the SR and SDS-SR adsorption capacities, highlighting an excellent agreement and a minimal prediction bias. This visible evidence supports the considerable R and R^2 values obtained previously in Table 3, confirming the accuracy of the ANN model in explaining and capturing complex adsorption patterns.

In figure S2.B the experimental data are successfully aligned with the ANN predicted values for both SR and SDS-SR biomasses. This confirms previous findings regarding the ability of the ANN model to accurately predict results and its capability to effectively represent and model the current adsorption system.

Fig. S2.C, illustrates the residuals for all sample and how the actual data values differ from their ANN predictions. Residuals are centered closely around zero, show no familiar pattern, indicating that the model errors are just random, and cannot be biased. The narrow difference between residuals also points to the low RMSE found for both biomasses shown in Table 3.

The error histogram (Fig. S2.D) explains the frequency distribution of prediction errors. It has been observed that most errors fall within a narrow range close to zero; this suggests the ANN model is very accurate. The distribution is symmetrical and bell-shaped, which means that the variations in ANN predictions are quite small.

3.13. Optimization of adsorption capacity using genetic algorithm and particle swarm optimization

In order to enhance the adsorption capacity of both SR and SDS-SR biomasses advanced optimization methods were applied, Genetic Algorithm (GA) and Particle Swarm Optimization (PSO), with a surrogate model based on an artificial neural network (ANN). In the beginning, the range of each input (contact time, adsorbent concentration, initial dye concentration, pH, and temperature) were defined for each adsorbent.

Referring to table 4, both GA and PSO provided the optimal parameters that resulted in the highest adsorption capacities. For SR, the results showed that both PSO and GA gave almost the same result, with adsorption of 56.09 mg/g for GA compared to 56.08 mg/g for PSO. When it comes to SDS-SR, the algorithms performed almost the same, as PSO predicted 99.56 mg/g and GA 99.36 mg/g. These findings agree with experiments and confirm the superior adsorption potential of SDS-treated biomass compared to the untreated SR biomass. In addition, these results highlight the benefits of integrating machine learning within optimization for predicting performance. In Summary, PSO and Genetic Algorithm shows almost similar performance, offering higher adsorption capacities for both SR and SDS-SR biomasses. Furthermore, the study proves that combining surrogate models with nature-inspired optimization is useful for guiding which tests to run, improving their efficiency, and support data-driven process development.

4. Conclusion

This study points out that the biomass of *Streptomyces rimosus* (SR) and its SDS-impregnated form (SDS-SR) have a promising potential as an effective, sustainable biosorbents for the removal of Fuchsin (BV14) from aqueous solutions. By reusing biomass generated by pharmaceutical companies, this solution handles waste and supports the beliefs of circular economy and green chemistry at the same time.

The surfactant treatment of biomass increases the material's adsorption performance. Compared to raw SR, the SDS-SR, was able to adsorb more than 98% of the dye using only half the absorbent dose, proving it has better surface and increased dye adsorbing ability. This improvement is attributed to the sulfate groups negatively charged attached to the biomass surface by SDS, which promoted both electrostatic and surface heterogeneity.

The adsorption mechanism meets the requirements of the pseudo-second-order model, which indicates that chemisorption process is the rate-determining step. The Hill and Sips isotherms provided the optimal description of equilibrium data, which confirms surface heterogeneity effects with cooperative adsorption binding and the potential development of multilayers.

Thermodynamic analysis indicated that the adsorption process at low temperature was spontaneous ($\Delta G^\circ < 0$) and exothermic ($\Delta H^\circ < 0$) for both biomasses with a slight decrease in spontaneity at higher temperatures. It is notable that SDS-SR exhibited more negative enthalpy ΔH° (−103.98 KJ/moL) and greater entropy decrease (ΔS°) which suggests that the dye-adsorbent interactions of SDS-SR are stronger than those of raw SR. These findings prove that the process is dominated by physisorption and reinforced by surface modification.

Reusing the biomass of *Streptomyces rimosus* over several cycles, with or without SDS treatment, proves its potential as a cost effective and sustainable adsorbent for wastewater treatment, despite a gradual decrease in efficiency due to the effects of regeneration.

The results of the DFT studies support and rationalize the experimental results by confirming that SDS modification doubles the adsorption energy of BV14, providing a mechanistic explanation for the greater capacity, faster equilibrium and more exothermic behavior of the SDS-SR biosorbent.

On the whole, this work confirms that reusing microbial waste biomass to remove dyes from wastewater is an inexpensive approach, and highlights the advantages and potential benefits of the SDS impregnation as a powerful strategy for improving the adsorption capacity, efficiency, and thermodynamic favorability. These findings prove that this system deserves consideration for future environmentally safe and practical wastewater treatments.

Additionally, the integration of artificial intelligence in biosorption research to build reliable models and optimize the adsorption performance. Among the ML models tested, the artificial neural network model predicted better the adsorption performance. Coupled with GA and PSO, the model enabled precise identification of optimal conditions, predicting even higher adsorption capacities than those observed experimentally. These results highlight the power of hybrid biosorption-AI approaches in the design of an efficient and a sustainable wastewater treatment system, offering a model for future smart environmental technologies.

CRediT authorship contribution statement

Amira Othmani: Writing – original draft, Methodology, Investigation, Formal analysis, Conceptualization. **Ibtissam Hammouche:** Writing – original draft, Software, Methodology, Data curation. **Ammar Selatnia:** Writing – review & editing, Validation, Project administration, Conceptualization. **Nasma Bouchelkia:** Writing – review & editing, Supervision, Methodology, Investigation.

Declaration of competing interest

The authors declare that they have no known competing financial interests or personal relationships that could have appeared to influence the work reported in this paper.

Appendix A. Supplementary data

Supplementary data to this article can be found online at https://doi.org/10.1016/j.wasman.2026.115470.

Data availability

Data will be made available on request.

References

Ahamad, Z., Nasar, A., 2024. Synthesis, characterization, and application of magnetized *Azadirachta indica* sawdust as a novel adsorbent: kinetic, and isotherm studies in removing methylene blue as a model dye. Cellul. 31, 3763–3782. https://doi.org/10.1007/s10570-024-05813-z.

Ahmad, W., Amin, Z., ur Rehman, T., Hussain, F., Ilyas, M.,, 2022. Treatment of dyes contaminated water using surfactants modified activated carbon derived from rice husk. Desalin. Water Treat. 248, 288–299. https://doi.org/10.5004/dwt.2022.28115.

Al-Maliky, E.A., Gzar, H.A., Al-Azawy, M.G., 2021. Determination of Point of Zero Charge (PZC) of Concrete Particles Adsorbents. IOP Conf. Ser.: Mater. Sci. Eng. 1184, 012004. https://doi.org/10.1088/1757-899x/1184/1/012004.

Alamin, N.U., Khan, A.S., Nasrullah, A., Iqbal, J., Ullah, Z., Din, I.U., Muhammad, N., Khan, S.Z., 2021. Activated carbon-alginate beads impregnated with surfactant as sustainable adsorbent for efficient removal of methylene blue. Int. J. Biol. Macromol. 176, 233–243. https://doi.org/10.1016/j.ijbiomac.2021.02.017.

Ali, B., Naceur, B., Abdelkader, E., Karima, E., Nourredine, B., 2022. Competitive adsorption of binary dye from aqueous solutions using calcined layered double hydroxides. Int. J. Environ. Anal. Chem. 102, 3207–3226. https://doi.org/10.1080/03067319.2020.1766035.

Almas, M., Khan, A.S., Nasrullah, A., Din, I.U., Fagieh, T.M., Bakhsh, E.M., Akhtar, K., Khan, S.B., Khan, S.Z., Inayat, A., 2023. Substantial increase in adsorption efficiency of local clay-alginate beads toward methylene blue impregnated with SDS. Environ. Sci. Pollut. Res. 30, 81433–81449. https://doi.org/10.1007/s11356-022-23949-y.

Alsaiari, N.S., Osman, H., Amari, A., Tahoon, M.A., 2022. The Synthesis of Metal–Organic-Framework-based Ternary Nanocomposite for the Adsorption of Organic Dyes from Aqueous Solutions. Magnetochemistry 8. https://doi.org/10.3390/magnetochemistry8100133.

Aminu, I., Gumel, S.M., Ahmad, W.A., Idris, A.A., 2020. Adsorption Isotherms and Kinetic Studies of Congo-Red Removal from Waste Water using Activated Carbon Prepared from Jujube seed. Am. J. Anal. Chem. 11, 47–59. https://doi.org/10.4236/ajac.2020.111004.

Amiri, M.J., Raayatpisheh, M., 2024. Adsorption behavior of cationic dyes on starch nanocrystals: Kinetic, isotherm, and thermodynamic insights from single to multi-component systems. Int. J. Biol. Macromol. 281, 136310. https://doi.org/10.1016/j.ijbiomac.2024.136310.

Asim, N., Badiei, M., Shakeri, M., Emdadi, Z., Samsudin, N.A., Soltani, S., Mohammad, M., Amin, N., 2022. Development of green photocatalytic geopolymers for dye removal. Mater. Chem. Phys. 283, 126020. https://doi.org/10.1016/j.matchemphys.2022.126020.

Azeez, R.A., Al-Zuhairi, F.K.I., 2022. Biosorption of dye by immobilized yeast cells on the surface of magnetic nanoparticles. Alexandria Eng. J. 61, 5213–5222. https://doi.org/10.1016/j.aej.2021.10.044.

Azoulay, K., Bencheikh, I., Mabrouki, J., Samghouli, N., Moufti, A., Dahchour, A., El Hajjaji, S., 2023. Adsorption mechanisms of azo dyes binary mixture onto different raw palm wastes. Int. J. Environ. Anal. Chem. 103, 1633–1652. https://doi.org/10.1080/03067319.2021.1878165.

Bat-Amgalan, M., Khashbaatar, Z., Anak, D.E.V., Sari, M.N.M., Miyamoto, N., Kano, N., Kim, H.-J., Yunden, G., 2021. Adsorption of Cr(III) from an Aqueous solution by Chitosan Beads Modified with Sodium Dodecyl Sulfate (SDS). J. Environ. Prot. (irvine, Calif) 12, 939–960. https://doi.org/10.4236/jep.2021.1211055.

Benazouz, K., Bouchelkia, N., Imessaoudene, A., Bollinger, J.-C., Amrane, A., Assadi, A. A., Zeghioud, H., Mouni, L., 2023. Efficient and Low-cost Water Remediation for Chitosan Derived from Shrimp Waste, an Ecofriendly Material: Kinetics Modeling, Response Surface Methodology Optimization, and Mechanism. Water. https://doi.org/10.3390/w15213728.

Benazouz, K., Bouchelkia, N., Moussa, H., Boutheldja, R., Zamouche, M., Amrane, A., Parvathiraja, C., Al-Lohedan, H.A., Bollinger, J.C., Mouni, L., 2025. Efficient Removal of Cu(II) from Wastewater using Chitosan Derived from Shrimp Shells: a Kinetic, Thermodynamic, Optimization, and Modelling Study. Water (switzerland) 17. https://doi.org/10.3390/w17060851.

Bharagava, R.N., Saxena, G., Mulla, S.I., 2020. In: Introduction to Industrial Wastes Containing Organic and Inorganic Pollutants and Bioremediation Approaches for Environmental Management BT - Bioremediation of Industrial Waste for Environmental Safety: Volume i: Industrial Waste and Its Management. Springer Singapore, Singapore, pp. 1–18. https://doi.org/10.1007/978-981-13-1891-7_1.

Bouchelkia, N., Benazouz, K., Mameri, A., Belkhiri, L., Hamri, N., Belkacemi, H., Zoukel, A., Amrane, A., Aoulmi, F., Mouni, L., 2023a. Study and Characterization of H3PO4 Activated Carbons Prepared from Jujube Stones for the Treatment of Industrial Textile Effluents. Processes 11. https://doi.org/10.3390/pr11092694.

Bouchelkia, N., Tahraoui, H., Amrane, A., Belkacemi, H., Bollinger, J.C., Bouzaza, A., Zoukel, A., Zhang, J., Mouni, L., 2023b. Jujube stones based highly efficient activated carbon for methylene blue adsorption: Kinetics and isotherms modeling, thermodynamics and mechanism study, optimization via response surface methodology and machine learning approaches. Process Saf. Environ. Prot. 170, 513–535. https://doi.org/10.1016/j.psep.2022.12.028.

Bouchelkia, N., Tahraoui, H., Benazouz, K., Mameri, A., Boudraa, R., Moussa, H., Hamri, N., Merdoud, R., Belkacemi, H., Zoukel, A., Amrane, A., Kebir, M., Mouni, L., 2025. Optimizing adsorption efficiency: a novel application of SVM_Boosting_IGWO for methylene blue dye removal using low-cost fruit peels adsorbents. Chemom. Intell. Lab. Syst. 261, 105377. https://doi.org/10.1016/j.chemolab.2025.105377.

Calisto, J.S., Pacheco, I.S., Freitas, L.L., Santana, L.K., Fagundes, W.S., Amaral, F.A., Canobre, S.C., 2019. Adsorption kinetic and thermodynamic studies of the 2, 4 - dichlorophenoxyacetate (2,4-D) by the [Co-Al-Cl] layered double hydroxide. Heliyon 5, e02553. https://doi.org/10.1016/j.heliyon.2019.e02553.

Chan, S.S., Khoo, K.S., Chew, K.W., Ling, T.C., Show, P.L., 2022. Recent advances biodegradation and biosorption of organic compounds from wastewater: Microalgae-bacteria consortium - a review. Bioresour. Technol. 344, 126159. https://doi.org/10.1016/j.biortech.2021.126159.

Chatterjee, S., Chatterjee, T., Lim, S.-R., Woo, S.H., 2011. Effect of surfactant impregnation into chitosan hydrogel beads formed by sodium dodecyl sulfate gelation for the removal of congo red. Sep. Sci. Technol. 46, 2022–2031.

Cheikh, S., Imessaoudene, A., Bollinger, J.-C., Hadadi, A., Manseri, A., Bouzaza, A., Assadi, A., Amrane, A., Zamouche, M., El Jery, A., Mouni, L., 2023. Complete Elimination of the Ciprofloxacin Antibiotic from Water by the Combination of Adsorption–Photocatalysis Process using Natural Hydroxyapatite and TiO2. Catalysts. https://doi.org/10.3390/catal13020336.

Dar, I.S., Chand, S., 2024. Bootstrap-quantile ridge estimator for linear regression with applications. PLoS One 19, e0302221.

Deyris, P.-A., Pelissier, F., Grison, C.M., Hesemann, P., Petit, E., Grison, C., 2023. Efficient removal of persistent and emerging organic pollutants by biosorption using abundant biomass wastes. Chemosphere 313, 137307. https://doi.org/10.1016/j.chemosphere.2022.137307.

Djebbah, F.Z., Al-Dhabi, N.A., Arasu, M.V., Belyagoubi, L., Kherbouche, F., Abdelouahid, D.E., Ravindran, B., 2022. Isolation and characterisation of Streptomyces sp. Strain GLD25 with antimicrobial and antioxidant effects from Gueldaman cave (GLD1). Akbou-Algeria. J. King Saud Univ. - Sci. 34, 101719. https://doi.org/10.1016/j.jksus.2021.101719.

do Nascimento Júnior, W.J., de Aguiar, G.H., Massarelli, R.C., Landers, R., Vieira, M.G. A., da Motta Sobrinho, M.A.,, 2024. Multi-pollutant biosorption of organic and inorganic pollutants by brown algae waste from alginate production: batch and fixed-bed investigation. Environ. Sci. Pollut. Res. 31, 53580–53597. https://doi.org/10.1007/s11356-023-30511-x.

Domingo, L.R., Sáez, J.A., Pérez, P., 2007. A comparative analysis of the electrophilicity of organic molecules between the computed IPs and EAs and the HOMO and LUMO energies. Chem. Phys. Lett. 438, 341–345. https://doi.org/10.1016/j.cplett.2007.03.023.

Ebelegi, A.N., Ayawei, N., Wankasi, D., 2020. Interpretation of Adsorption Thermodynamics and Kinetics. Open J. Phys. Chem. 10, 166–182. https://doi.org/10.4236/ojpc.2020.103010.

El-Sayed, E., El-Aziz, E.A., Othman, H.A., Hassabo, A.G., 2024. Azo dyes: Synthesis, Classification and Utilisation in Textile Industry. Egypt. J. Chem. 67, 87–97. 10.21608/ejchem.2024.257952.9057.

Elgarahy, A.M., Elwakeel, K.Z., Mohammad, S.H., Elshoubaky, G.A., 2021. A critical review of biosorption of dyes, heavy metals and metalloids from wastewater as an efficient and green process. Clean. Eng. Technol. 4, 100209. https://doi.org/10.1016/j.clet.2021.100209.

Feddane, S., Oukebdane, K., Didi, M.A., Didi, A., Amara, A., Larabi, O., 2023. Removal of textile dye Bemacid Red from water using *Casuarina equisetifolia* needles: kinetic and thermodynamic modeling. Desalin. Water Treat. 289, 248–257. https://doi.org/10.5004/dwt.2023.29403.

Finlay, A.C., Hobby, G.L., P'an, S.Y., Regna, P.P., Routien, J.B., Seeley, D.B., Shull, G.M., Sobin, B.A., Solomons, I.A., Vinson, J.W., Kane, J.H., 1950. Terramycin, a new antibiotic. Science (80-.). 111, 85. https://doi.org/10.1126/science.111.2874.85.a.

Gad, A.G., 2022. Particle swarm optimization algorithm and its applications: a systematic review. Arch. Comput. Meth. Eng. 29, 2531–2561.

Gamboa, D.M., Abatal, M., Lima, E., Franseschi, F.A., Ucán, C.A., Tariq, R., Elías, M.A., Vargas, J., 2024. Sorption Behavior of Azo Dye Congo Red onto Activated Biochar from Haematoxylum campechianum Waste: Gradient Boosting Machine Learning-

Assisted Bayesian Optimization for improved Adsorption Process. Int. J. Mol. Sci. https://doi.org/10.3390/ijms25094771.
Ghosh, N., Sen, S., Biswas, G., Saxena, A., Haldar, P.K., 2023. Adsorption and Desorption Study of Reusable magnetic Iron Oxide Nanoparticles Modified with Justicia adhatoda Leaf Extract for the Removal of Textile Dye and Antibiotic. Water Air Soil Pollut. 234. https://doi.org/10.1007/s11270-023-06217-8.
Goldberg, S., Criscenti, L.J., Turner, D.R., Davis, J.A., Cantrell, K.J., 2007. Adsorption–desorption processes in subsurface reactive transport modeling. Vadose Zo. J. 6, 407–435.
Grigoraș, C.G., Simion, A.I., Favier, L., Drob, C., Gavrilă, L., 2022. Performance of Dye Removal from Single and Binary Component Systems by Adsorption on Composite Hydrogel Beads Derived from Fruits Wastes Entrapped in Natural Polymeric Matrix. Gels 8. https://doi.org/10.3390/gels8120795.
Guleria, A., Kumari, G., Lima, E.C., Ashish, D.K., Thakur, V., Singh, K., 2022. Removal of inorganic toxic contaminants from wastewater using sustainable biomass: a review. Sci. Total Environ. 823, 153689. https://doi.org/10.1016/j.scitotenv.2022.153689.
Guo, Y., Li, G., Xiao, Z., Li, F., Cheng, F., Zhao, Z., Guo, S., 2024. Effect of Electrokinetic Leaching with Surfactant on Desorption of Semi-Volatile Organic Pollutants in Soil. Water Air Soil Pollut. 235, 611.
Hamri, N., Ali, I., Nasma, B., Reguia, B., Sabrina, C., Jean-Claude, B., Aymen Amine, A., Abdelhamid, B., Mouni, L., 2024. Innovative surface modification of Kaolinite by direct grafting of an anionic surfactant to improve pollutant adsorption and effluent decontamination. J. Dispers. Sci. Technol. 1–20. https://doi.org/10.1080/01932691.2024.2448761.
Hamri, N., Imessaoudene, A., Bouchelkia, N., Boudraa, R., Cheikh, S., Bollinger, J.C., Assadi, A.A., Boukerroui, A., Mouni, L., 2025. Innovative surface modification of Kaolinite by direct grafting of an anionic surfactant to improve pollutant adsorption and effluent decontamination. J. Dispers. Sci. Technol. 1–20. https://doi.org/10.1080/01932691.2024.2448761.
Hassan, R., Kazemi, M.R., 2025. Machine learning frameworks to accurately estimate the adsorption of organic materials onto resin and biochar. Sci. Rep. 15, 15157. https://doi.org/10.1038/s41598-025-99759-2.
Ho, Y.S., Mckay, G., 1999. Pseudo-second order model for sorption processes. Process Biochem. 34, 451–465. https://doi.org/10.1016/S0032-9592(98)00112-5.
Ibrahim, S.M., Al-Harby, N.F., El-Molla, S.A., Ibrahim, E.-S., 2024. New combined experimental and DFT studies for adsorption of sole Azo-dye or binary cationic dyes from aqueous solution. Sci. Rep. 14, 14756. https://doi.org/10.1038/s41598-024-65649-2.
Islam, Touhidul, Islam, Tarekul, Islam, Tarikul, Repon, R., 2022. Synthetic Dyes for Textile Colouration: Process, Factors and Environmental Impact. Text. Leather Rev. 5, 327–373. 10.31881/TLR.2022.27.
Ismail, F.N., Rahim, A.R.A., Abd Aziz, M.A.Z., Johari, K., 2025. Experimental and isotherm modelling process of lead (II) adsorption on silica nanocapsule adsorbents, in. Journal of Physics: Conference Series. IOP Publishing 12035.
Griffiths, J., 1984. Developments in the light absorption properties of dyes-color and photochemical reactions. Soc. Chem. Ind. 1–30.
Jasri, K., Abdulhameed, A.S., Jawad, A.H., ALOthman, Z.A., Yousef, T.A., Al Duaij, O.K.,, 2023. Mesoporous activated carbon produced from mixed wastes of oil palm frond and palm kernel shell using microwave radiation-assisted K2CO3 activation for methylene blue dye removal: Optimization by response surface methodology. Diam. Relat. Mater. 131, 109581. https://doi.org/10.1016/j.diamond.2022.109581.
Jawad, A.H., Ismail, K., Ishak, M.A.M., Wilson, L.D., 2019. Conversion of Malaysian low-rank coal to mesoporous activated carbon: Structure characterization and adsorption properties. Chinese J. Chem. Eng. 27, 1716–1727. https://doi.org/10.1016/j.cjche.2018.12.006.
Jaymand, M., 2024. Biosorptive removal of cationic dyes from ternary system using a magnetic nanocomposite hydrogel based on modified tragacanth gum. Carbohydr. Polym. Technol. Appl. 7, 100403. https://doi.org/10.1016/j.carpta.2023.100403.
Katoch, S., Chauhan, S.S., Kumar, V., 2021. A review on genetic algorithm: past, present, and future. Multimed. Tools Appl. 80, 8091–8126.
Khan, K.A., Shah, A., Nisar, J., Haleem, A., Shah, I., 2023. Photocatalytic Degradation of Food and Juices Dyes via Photocatalytic Nanomaterials Synthesized through Green Synthetic Route: a Systematic Review. Molecules. https://doi.org/10.3390/molecules28124600.
Khiam, G.K., Karri, R.R., Mubarak, N.M., Khalid, M., Walvekar, R., Abdullah, E.C., Rahman, M.E., 2022. Modelling and optimization for methylene blue adsorption using graphene oxide/chitosan composites via artificial neural network-particle swarm optimization. Mater. Today Chem. 24, 100946. https://doi.org/10.1016/j.mtchem.2022.100946.
Kim, S., Chen, J., Cheng, T., Gindulyte, A., He, J., He, S., Li, Q., Shoemaker, B.A., Thiessen, P.A., Yu, B., Zaslavsky, L., Zhang, J., Bolton, E.E., 2025. PubChem 2025 update. Nucleic Acids Res. 53, D1516–D1525. https://doi.org/10.1093/nar/gkae1059.
Kirova, G., Velkova, Z., Stoytcheva, M., Gochev, V., 2021. Tetracycline removal from model aqueous solutions by pretreated waste *Streptomyces fradiae* biomass. Biotechnol. Biotechnol. Equip. 35, 953–963. https://doi.org/10.1080/13102818.2021.1938677.
Kooh, M.R.R., Dahri, M.K., Lim, L.B.L., Lim, L.H., Lee, S.L., 2019. Phytoextraction capability of Azolla pinnata in the removal of rhodamine B from aqueous solution: artificial neural network and random forests approaches. Appl Water Sci 9, 1–9. https://doi.org/10.1007/s13201-019-0960-6.
Kooh, M.R.R., Lim, L.B.L., Lim, L.H., Bandara, J.M.R.S., 2016. Batch adsorption studies on the removal of malachite green from water by chemically modified Azolla pinnata. Desalin. Water Treat. 57, 14632–14646. https://doi.org/10.1080/19443994.2015.1065450.
Kooh, M.R.R., Linda, B.L., L., Lee-Hoon, L., and Malik, O.A.,, 2018. Phytoextraction potential of water fern (Azolla pinnata) in the removal of a hazardous dye, methyl violet 2B: Artificial neural network modelling. Int. J. Phytorem. 20, 424–431. https://doi.org/10.1080/15226514.2017.1365337.
Lagergren, S., 1898. About the theory of so-called adsorption of soluble substances. K. Sven. Vetenskapsakademies Handl. 24, 1–39.
Li Haksun, P., 2022. Introduction to Numerical Methods in Java, in: Numerical Methods Using Java: For Data Science, Analysis, and Engineering. Springer, pp. 1–69.
Li, C., Ye, F., Chahine, R., Yang, T., Xiao, J., 2024a. Genetic algorithm optimized artificial neural network models of single- and multi-component gas adsorption isotherms for hydrogen purification. Int. J. Hydrogen Energy 52, 1127–1142. https://doi.org/10.1016/j.ijhydene.2023.04.352.
Li, J., Lin, G., Zhong, Z., Wang, Z., Wang, S., Fu, L., Hu, T., 2024b. A novel magnetic Ti-MOF/chitosan composite for efficient adsorption of Pb(II) from aqueous solutions: Synthesis and investigation. Int. J. Biol. Macromol. 258, 129170. https://doi.org/10.1016/j.ijbiomac.2023.129170.
Mabuza, M.M., Mahlobo, M.G.R., 2025. Adsorption Equilibria and Systematic Thermodynamics Analysis of Carbon Dioxide Sequestration on South African Coals using Nonlinear Three-Parameter Models: Sips, Tóth, and Dubinin–Astakhov. Energies 18, 1–20. https://doi.org/10.3390/en18102646.
Madhuranthakam, C.M.R., Hourfar, F., Elkamel, A., 2024. Artificial neural network modeling in the presence of uncertainty for predicting hydrogenation degree in continuous nitrile butadiene rubber processing. Processes 12, 999.
Mostoufi, N., Constantinides, A., 2023. Linear and nonlinear regression analysis. Appl. Numer. Methods Chem. Eng. Katey Birtcher; Merken, S., Ed 403–476.
Nandiyanto, A.B.D., Nugraha, W.C., Yustia, I., Ragadhita, R., Fiandini, M., Meirinawati, H., Wulan, D.R., 2024. Isotherm and kinetic adsorption of rice husk particles as a model adsorbent for solving issues in the sustainable gold mining environment from mercury leaching. J. Min. Inst. 104–120.
Naseem, K., Ali, F., Tahir, M.H., Afaq, M., Yasir, H.M., Ahmed, K., Aljuwayid, A., muteb, Habila, M.A.,, 2022. Investigation of catalytic potential of sodium dodecyl sulfate stabilized silver nanoparticles for the degradation of methyl orange dye. J. Mol. Struct. 1262, 132996. https://doi.org/10.1016/j.molstruc.2022.132996.
Nebaghe, K.C., El Boundati, Y., Ziat, K., Naji, A., Rghioui, L., Saidi, M., 2016. Comparison of linear and non-linear method for determination of optimum equilibrium isotherm for adsorption of copper(II) onto treated Martil sand. Fluid Phase Equilib. 430, 188–194. https://doi.org/10.1016/j.fluid.2016.10.003.
Obayomi, K.S., Lau, S.Y., Zahir, A., Meunier, L., Zhang, J., Dada, A.O., Rahman, M.M., 2023. Removing methylene blue from water: a study of sorption effectiveness onto nanoparticles-doped activated carbon. Chemosphere 313, 137533.
Okoro, H.K., Pandey, S., Ogunkunle, C.O., Ngila, C.J., Zvinowanda, C., Jimoh, I., Lawal, I.A., Orosun, M.M., Adeniyi, A.G., 2022. Nanomaterial-based biosorbents: Adsorbent for efficient removal of selected organic pollutants from industrial wastewater. Emerg. Contam. 8, 46–58. https://doi.org/10.1016/j.emcon.2021.12.005.
Ormachea, C.M., Mancini, P.M.E., Kneeteman, M.N., Domingo, L.R., 2015. Understanding the participation of 3-nitropyridine in polar Diels–Alder reactions. A DFT Study. Comput. Theor. Chem. 1072, 37–42. https://doi.org/10.1016/j.comptc.2015.08.024.
Othmani, A., Hammouche, I., Selatnia, A., 2026. From batch to fixed-bed biosorption of Congo red using surfactant-modified wood chips: Mechanistic insights, regeneration, real wastewater validation and machine-learning modelling. J. Environ. Manage. 399, 128613. https://doi.org/10.1016/j.jenvman.2026.128613.
Othmani, A., Selatnia, A., Hamitouche, A., Bachari, K., 2025. Sustainable biosorption of cationic textile dyes (BY28, BB41, BR46) from aqueous solutions using pharmaceutical waste biomass (*Streptomyces rimosus*): Comparative study in single, binary, and ternary systems. J. Water Process Eng. 76, 108103. https://doi.org/10.1016/j.jwpe.2025.108103.
Patil, R., Zahid, M., Govindwar, S., Khandare, R., Vyavahare, G., Gurav, R., Desai, N., Pandit, S., Jadhav, J., 2022. Chapter 8 - Constructed wetland: a promising technology for the treatment of hazardous textile dyes and effluent, in: Shah, M., Rodriguez-Couto, S., Biswas, J.B.T.-D. in W.T.R. and P. (Eds.), . Elsevier, pp. 173–198. 10.1016/B978-0-323-85583-9.00016-8.
Que, W., Jiang, L., Wang, C., Liu, Y., Zeng, Z., Wang, X., Ning, Q., Liu, S., Zhang, P., Liu, S., 2018. Influence of sodium dodecyl sulfate coating on adsorption of methylene blue by biochar from aqueous solution. J. Environ. Sci. 70, 166–174. https://doi.org/10.1016/j.jes.2017.11.027.
Rad, A.S., Ardjmand, M., Esfahani, M.R., Khodashenas, B., 2021. DFT calculations towards the geometry optimization, electronic structure, infrared spectroscopy and UV-vis analyses of Favipiravir adsorption on the first-row transition metals doped fullerenes; a new strategy for COVID-19 therapy. Spectrochim. Acta A Mol. Biomol. Spectrosc. 247, 119082. https://doi.org/10.1016/j.saa.2020.119082.
Ranjbari, S., Ayati, A., Tanhaei, B., Al-Othman, A., Karimi, F., 2022. The surfactant-ionic liquid bi-functionalization of chitosan beads for their adsorption performance improvement toward Tartrazine. Environ. Res. 204, 111961. https://doi.org/10.1016/j.envres.2021.111961.
Sahnoun, A.Y., Selatnia, A., Mitu, L., Ayeche, R., Daoud, N., Dahoun-Tchoulak, Y., 2024. Basic Red 46 adsorption studies onto pyrolyzed by-product biomass. Appl Water Sci 14, 1–16. https://doi.org/10.1007/s13201-024-02150-1.
Sandollah, N.A.S.M., Ghazali, S.A.I.S.M., Ibrahim, W.N.W., Rusmin, R., 2020. Adsorption-desorption profile of methylene blue dye on raw and acid activated kaolinite. Indones. J. Chem. 20, 755–765.
Sassi, W., Msaadi, R., Ardhaoui, N., Ammar, S., Nafady, A., 2023. Selective/simultaneous batch adsorption of binary textile dyes using amorphous perlite powder: aspects of central composite design optimization and mechanisms. J. Environ. Heal. Sci. Eng. 21, 441–454. https://doi.org/10.1007/s40201-023-00870-1.

Saxena, N., Islam, M.M., Baliyan, S., Sharma, D., 2023. A comprehensive review on removal of environmental pollutants using a surfactant based remediation process. RSC Sustain. 1, 2148–2161.
Sharma, R., Agrawal, P.R., Kumar, R., Ittishree, Gupta, G., 2022. Biosorption for Eliminating Inorganic Contaminants (IOCs) from Wastewater, in: Biosorption for Wastewater Contaminants. pp. 42–62. 10.1002/9781119737629.ch3.
Sharma, R., Pravin Kumar, K., Dash, S., 2024. Correlating solvation-adsorption phenomena of some styrylpyridinium dyes on SDS modified silica surface in organic media. J. Dispers. Sci. Technol. 45, 548–558. https://doi.org/10.1080/01932691.2022.2161562.
Sharma, S., Ezung, S., Supong, A., Baruah, M., Kumar, S., Umdor, R., Sinha, D., 2023. Activated carbon adsorbent derived from waste biomass, "Croton caudatus" for efficient removal of 2-chlorophenol from aqueous solution: Kinetics, isotherm, thermodynamics and DFT simulation. Chem. Eng. Res. Des. 190. https://doi.org/10.1016/j.cherd.2023.01.002.
Shefer, I., Lopez, K., Straub, A.P., Epsztein, R., 2022. Applying Transition-State Theory to Explore Transport and Selectivity in Salt-Rejecting Membranes: a critical Review. Environ. Sci. Technol. 56, 7467–7483. https://doi.org/10.1021/acs.est.2c00912.
K. Singha P. Pandit S. Maity S.R. Sharma Chapter 11 - Harmful environmental effects for textile chemical dyeing practice N. Ibrahim C.-M.-B.-T.-.-G.-C. Hussain . for S.T. The Textile Institute Book Series 2021 Woodhead Publishing 153 164 10.1016/B978-0-323-85204-3.00005-1.
Sintakindi, A., Ankamwar, B., 2021. Fungal biosorption as an alternative for the treatment of dyes in waste waters: a review. Environ. Technol. Rev. 10, 26–43. https://doi.org/10.1080/21622515.2020.1869322.
Sivarajasekar, N., Baskar, R., 2019. Adsorption of Basic Magenta II onto H2SO4 activated immature *Gossypium hirsutum* seeds: Kinetics, isotherms, mass transfer, thermodynamics and process design. Arab. J. Chem. 12, 1322–1337. https://doi.org/10.1016/j.arabjc.2014.10.040.
Slama, H.B., Bouket, A.C., Pourhassan, Z., Alenezi, F.N., Silini, A., Cherif-Silini, H., Oszako, T., Luptakova, L., Golińska, P., Belbahri, L., 2021. Diversity of synthetic dyes from textile industries, discharge impacts and treatment methods. Appl. Sci. 11, 1–21. https://doi.org/10.3390/app11146255.
Sorour, F.H., Marouf, Y.M., Abd-elmonem, N.M., Mansour, R.A., 2023. Raw sawdust utilization for the removal of acid red57 and basic fuchsin dyes from aqueous solution : equilibrium , kinetics , and thermodynamic investigati. Int. J. Phytorem. 1–15. https://doi.org/10.1080/15226514.2023.2259999.
Supriya, S., Bhat, V.S., Jayeoye, T.J., Rujiralai, T., Chong, K.F., Hegde, G., 2022. An investigation on temperature-dependant surface properties of porous carbon nanoparticles derived from biomass. J. Nanostructure Chem. 12, 495–511. https://doi.org/10.1007/s40097-021-00427-4.
Tang, K.H.D., Darwish, N.M., Alkahtani, A.M., AbdelGawwad, M.R., Karácsony, P., 2022. Biological Removal of Dyes from Wastewater: a Review of its Efficiency and advances. Trop. Aquat. Soil Pollut. 2, 59–75. https://doi.org/10.53623/tasp.v2i1.72.
Tao, Z., Yang, Y., Hammes-Schiffer, S., 2019. Multicomponent density functional theory: including the density gradient in the electron-proton correlation functional for hydrogen and deuterium. J. Chem. Phys. 151. https://doi.org/10.1063/1.5119124.
Taoufik, N., Boumya, W., Elmoubarki, R., Elhalil, A., Achak, M., Abdennouri, M., Barka, N., 2022. Experimental design, machine learning approaches for the optimization and modeling of caffeine adsorption. Mater. Today Chem. 23, 100732. https://doi.org/10.1016/j.mtchem.2021.100732.
Tealab, A., 2018. Time series forecasting using artificial neural networks methodologies: a systematic review. Futur. Comput. Informatics J. 3, 334–340.
Tran, H.N., Lima, E.C., Juang, R.-S., Bollinger, J.-C., Chao, H.-P., 2021. Thermodynamic parameters of liquid–phase adsorption process calculated from different equilibrium constants related to adsorption isotherms: a comparison study. J. Environ. Chem. Eng. 9, 106674. https://doi.org/10.1016/j.jece.2021.106674.
Vanasundari, K., Balachandran, V., Kavimani, M., Narayana, B., 2017. Spectroscopic investigation, vibrational assignments, Fukui functions, HOMO-LUMO, MEP and molecular docking evaluation of 4 – [(3, 4 – dichlorophenyl) amino] 2 – methylidene 4 – oxo butanoic acid by DFT method. J. Mol. Struct. 1147, 136–147. https://doi.org/10.1016/j.molstruc.2017.06.096.
Wang, C., Du, J., Fan, X., 2022. High-dimensional correlation matrix estimation for general continuous data with Bagging technique. Mach. Learn. 111, 2905–2927.
Wang, T., Tang, J., Xia, H., Aljerf, L., Zhang, R., Tian, H., Akele, M.L., 2024. Intelligent optimal control of furnace temperature for the municipal solid waste incineration process using multi-loop controller and particle swarm optimization. Expert Syst. Appl. 257, 125015.
Wu, B., 1992. An introduction to neural networks and their applications in manufacturing. J. Intell. Manuf. 3, 391–403.
Xia, H., Tang, J., Aljerf, L., Chen, J., 2024. Unveiling dioxin dynamics: a whole-process simulation study of municipal solid waste incineration. Sci. Total Environ. 954, 176241.
Xu, R., Liu, J., Sun, W., Wang, L., 2023. Insights into the synergistic adsorption mechanism of mixed SDS/DDA collectors on biotite using quartz crystal microbalance with dissipation. Sep. Purif. Technol. 310, 123049.
Yang, H., Huang, K., Zhang, K., Weng, Q., Zhang, H., Wang, F., 2021. Predicting Heavy Metal Adsorption on Soil with Machine Learning and Mapping Global distribution of Soil Adsorption Capacities. Environ. Sci. Technol. 55, 14316–14328. https://doi.org/10.1021/acs.est.1c02479.
Yen, T.-W., Lim, T.-L., Yoon, T.-L., Lai, S.K., 2017. Studying the varied shapes of gold clusters by an elegant optimization algorithm that hybridizes the density functional tight-binding theory and the density functional theory. Comput. Phys. Commun. 220, 143–149. https://doi.org/10.1016/j.cpc.2017.07.002.
Yin, H.-M., Chen, K., Meštrović, R., Oliveira, T.A., 2022. on Statistics, Applied Mathematics, and Computing Science (CSAMCS 2021). In: Proc. of SPIE Vol.
Yılmaz, M., 2025. Comprehensive DFT study of 3-(2-furyl)-1 H-pyrazole-5-carboxylic acid: structural, spectroscopic, and electronic properties with optoelectronic implications. Sci. Rep. 15, 21983. https://doi.org/10.1038/s41598-025-05803-6.
Zeng, Z.-Y., Wang, Y.-S., Chao, S.D., 2017. Hydrogen bonded dimers of small alkyl substituted amides: Structures, energetics, and spectral analyses based on density functional theory calculations. Comput. Theor. Chem. 1113, 1–7. https://doi.org/10.1016/j.comptc.2017.05.004.
Zhang, Z., Gao, C., Chen, H., Zhang, X., Tan, C., Gong, Y., Bai, X., Zhang, Y., Li, H., 2024. The investigation of sorption–desorption performance and mechanism of copper by surfactant-modified zeolite in aqueous solutions. Environ. Sci. Pollut. Res. 31, 22962–22975.
Zhao, S., Chen, K., Xiong, B., Guo, C., Dang, Z., 2024. Prediction of adsorption of metal cations by clay minerals using machine learning. Sci. Total Environ. 924, 171733. https://doi.org/10.1016/j.scitotenv.2024.171733.
Zhao, Y.H., Geng, J.T., Cai, J.C., Cai, Y.F., Cao, C.Y., 2020. Adsorption performance of basic fuchsin on alkali-activated diatomite. Adsorpt. Sci. Technol. 38, 151–167. https://doi.org/10.1177/0263617420922084.